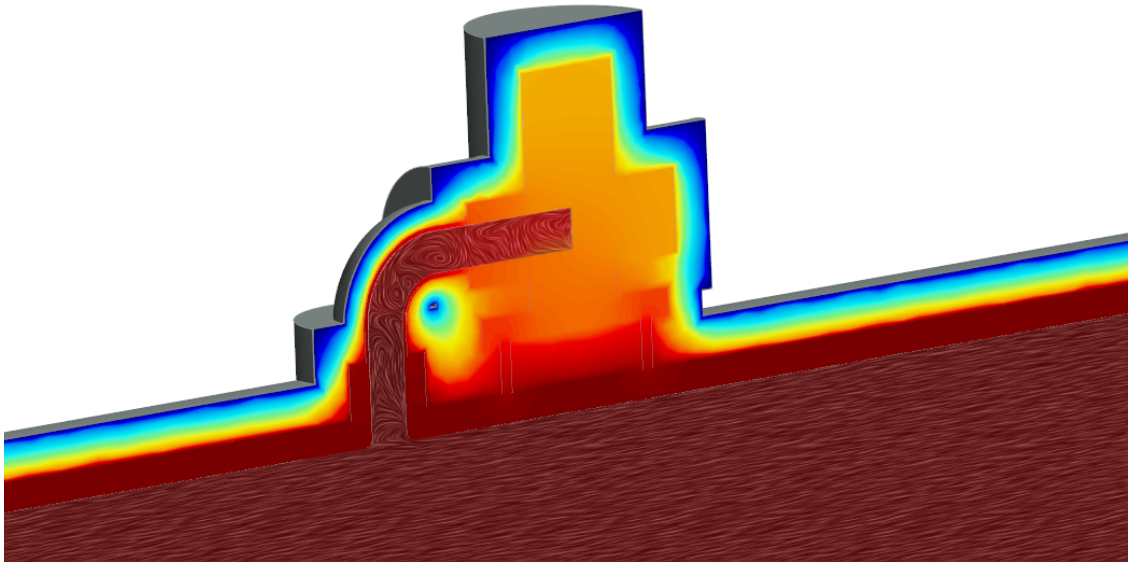

Hydrate Formation in Small Bore Dead Legs in Subsea Processing Systems

Master's thesis in Applied Mechanics

MAX BERGSTRÖM
JESPER PERSSON

DEPARTMENT OF MECHANICS AND MARITIME SCIENCES

CHALMERS UNIVERSITY OF TECHNOLOGY
Gothenburg, Sweden 2022
www.chalmers.se

Master's thesis in applied mechanics

Hydrate Formation in Small Bore Dead Legs in Subsea Processing Systems

MAX BERGSTRÖM
JESPER PERSSON

CHALMERS
UNIVERSITY OF TECHNOLOGY

Department of Mechanics and Maritime Sciences
Division of Fluid Dynamics
Chalmers University of Technology
Gothenburg, Sweden 2022

Hydrate Formation in Small Bore Dead Legs in Subsea Processing Systems
MAX BERGSTRÖM
JESPER PERSSON

Supervisor: Andrew Grant, Aker Solutions AS
Examiner: Henrik Ström, Department of Mechanics and Maritime Sciences

Master's Thesis 2022
Department of Mechanics and Maritime Sciences
Division of Fluid Dynamics
Chalmers University of Technology
SE-412 96 Gothenburg
Telephone +46 31 772 1000

Cover: Temperature field and flow structure visualization in a hydrocarbon displacement dead leg.

Typeset in LaTeX
Printed by Chalmers Reproservice
Gothenburg, Sweden 2022

Hydrate Formation in Small Bore Dead Legs in Subsea Processing Systems
MAX BERGSTRÖM
JESPER PERSSON
Department of Mechanics and Maritime Sciences
Chalmers University of Technology

Abstract

Natural gas hydrates, a crystalline compound forming at high pressures and low temperatures, pose flow assurance issues in natural gas processing systems. Small bore dead legs, piping containing stagnant process fluid, are prone to blocking by hydrate formation. This thesis aims to provide design guidelines and best practices for small bore dead leg design in natural gas subsea processing systems as well as providing a method for predicting hydrate thickness using computational fluid dynamics (CFD). An experiment which measured the final thickness of a hydrate in controlled conditions is recreated in CFD using three different approaches. One approach, volume of fluid (VOF) melting-solidification, shows promise with similar results to the experiment but with varying accuracy. Recommendations for future work on steady-state hydrate modelling in CFD are given. The small bore dead leg designs are evaluated from a conservative standpoint using CFD with the aim to provide general guidelines for a wide range of use cases in terms of process fluid composition, operating conditions and dead leg bore size. Design guidelines are given for common small bore dead leg functions, namely hydrocarbon displacement and mono-ethylene glycol injection. Guidelines for maximum and minimum small bore dead leg lengths are given for simple design geometries, such as straight pieces of piping. More geometrically complex designs are evaluated with respect to hydrate blocking from a thermal point of view. The guidelines and evaluated designs provide constraints and pre-verified solutions for future small bore dead leg designs regarding hydrate blocking mitigation.

Keywords: Natural gas, hydrates, CFD, subsea, dead leg.

Acknowledgements

The authors would like to express their sincere gratitude to our supervisor Andrew Grant. For his answers to all our questions and patience when explaining chemistry to mechanical engineers. A special thanks should also be directed to the people in the Aker Solutions Gothenburg office for showing interest in the work as well as engaging in discussions. The authors would also like to thank all the people who, in any capacity, have been involved in the work for their time and guidance. Last but not least, we would like to thank Henrik Alfredsson for giving us the opportunity to write this thesis.

Max Bergström and Jesper Persson, Gothenburg, June 2022

List of Acronyms

Below is the list of acronyms that have been used throughout this thesis listed in alphabetical order:

CFD	Computational Fluid Dynamics
EHTC	External Heat Transfer Coefficient
HC	Hydrocarbons
HCD	Hydrocarbon Displacement
HFT	Hydrate Formation Temperature
IHTC	Internal Heat Transfer Coefficient
MEG	Mono-Ethylene Glycol
OHTC	Overall Heat Transfer Coefficient
PTT	Pressure-Temperature Transducer
ROV	Remotely Operated Vehicle

Contents

List of Figures

List of Tables

1
Introduction

Natural gas is an important and reliable element in energy production systems around the world. Specifically it offers an opportunity for countries which historically have been reliant on energy from coal to significantly reduce their carbon emissions in line with common net-zero by 2050 targets. By comparison energy from natural gas emits 50-60% less carbon dioxide per kWh of produced electricity compared to coal [1]. Many of the regions that are reliant on energy from coal and oil, such as south east Asia, are also rich in natural gas. The energy demand in these regions is increasing fast, making the energy transition to renewables an even greater challenge. In fact, many countries with vast population centers still plan to increase their energy production from coal and oil [2]. When not correctly managed, coal-based emissions from these regions will vastly outpace the efforts of the developed world towards 2050 targets. Power generation from natural gas in combination with a step change towards solar and wind quickly needs to out compete coal. Recent changes in EU carbon taxonomy, labelling natural gas as a green investment [3], showcase a will by legislators to move in this direction at least in the short term. Improving the business case of natural gas production while also reducing emissions is essential to be successful in this task.

When producing natural gas, a mixture of gaseous hydrocarbons, water and hydrocarbon condensate is extracted from the well and flows through the production system [4]. This mixture of components has flow assurance challenges under conditions where hydrates can form blockages in the system. Natural gas hydrates are a solid crystalline compounds formed in presence of water and smaller guest molecules, usually hydrocarbons. The water molecules in contact with the guest molecule form a cage that traps the guest molecule. These cages in turn can form crystal lattices which constitut the hydrate [5]. In order for this reaction to occur the gas-water mixture must be maintained below the hydrate dissociation temperature for a sustained amount of time. The hydrate dissociation temperature is dependent on the molecular composition of the system as well as the pressure. In general an increased pressure and/or reduced temperature will heighten the risk for hydrate formation. Figure 1.1 shows how the hydrate dissociation temperature varies with pressure for an imaginary gas/condensate system forming the hydrate curve for that particular system.

An area of significant concern for hydrate formation is piping with stagnant process fluid called dead legs, where the process fluid risks losing heat over longer periods of time [6]. Dead legs can have a variety of functions and geometries. The design is generally influenced by what kind of system the dead leg is a part of. The dead legs in subsea production systems will be investigated in this thesis.

Subsea production systems consist of equipment placed subsea for production of oil and gas.

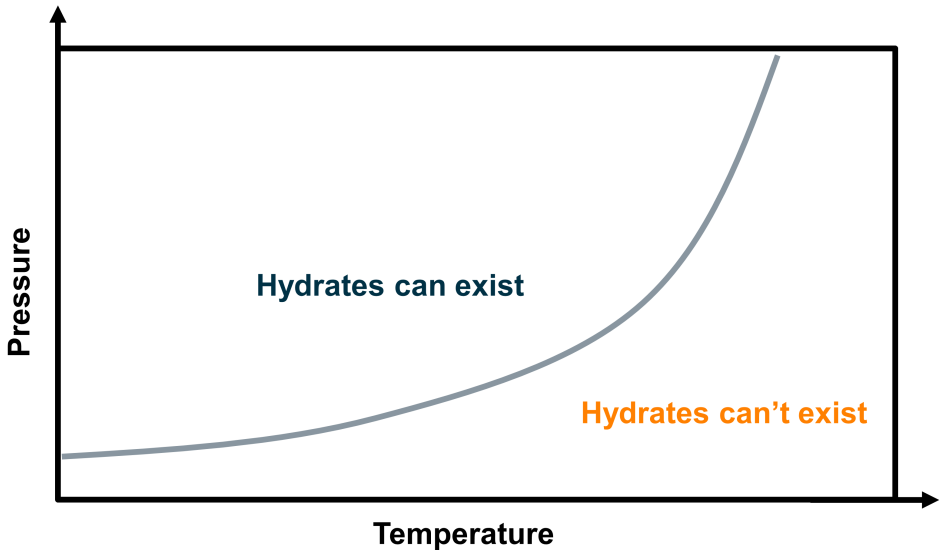

Figure 1.1: Hydrate curve for a typical gas/water mixture

This includes for example subsea christmas trees, which controls the production rate out of the well, and manifolds which combines production from several wells. One subset of subsea production systems is subsea processing systems, which can be defined as "any handling and treatment of the produced fluids for mitigating flow assurance issues prior to reaching the platform or onshore." [7]. It has the potential to make smaller and more remote fields with long tie-backs profitable while also extending the life of existing fields. One type of subsea processing is subsea gas compression, which allows for a more efficient extraction of natural gas by placing compressors on the seabed near the well. This effectively decreases the pressure drop downstream of the compression system [7]. By introducing compression to a gas field, the production life of the field is extended, and by placing the compressors on the seabed the compression power required is much less than what is required for a conventional topside compression system.

Subsea production systems are complex facilities that require numerous small bore connections into the large bore process pipes. These small bore connections allow many functions to be performed throughout the subsea production system, including chemical injection, hydrocarbon displacement, seawater displacement, and pressure and temperature monitoring. A significant amount of these small bore pipes are not in use during normal operation. This leads to the presence of a dead leg up to the first valve or instrument in the small bore pipe. These dead legs are of particular concern subsea as the cold seabed environment means operation near hydrate dissociation temperatures are more likely and they are therefore prone to hydrate formation. Subsea compression systems are especially prone to hydrate formation since they are operating at elevated pressures.

Due to remotely operated vehicle (ROV) access, stiffness or other conflicting requirements the simple solution to put the valve/instrument right at the connection to the large bore pipe (thereby minimizing the length of the dead leg) is not always possible. A schematic of what this piping could look like can be seen in figure 1.2. The small bore connections must therefore

be designed for hydrate prevention and mitigation to ensure the functionality of the processing system. If hydrates are allowed to form they risk plugging the dead leg, resulting in production loss or safety hazards.

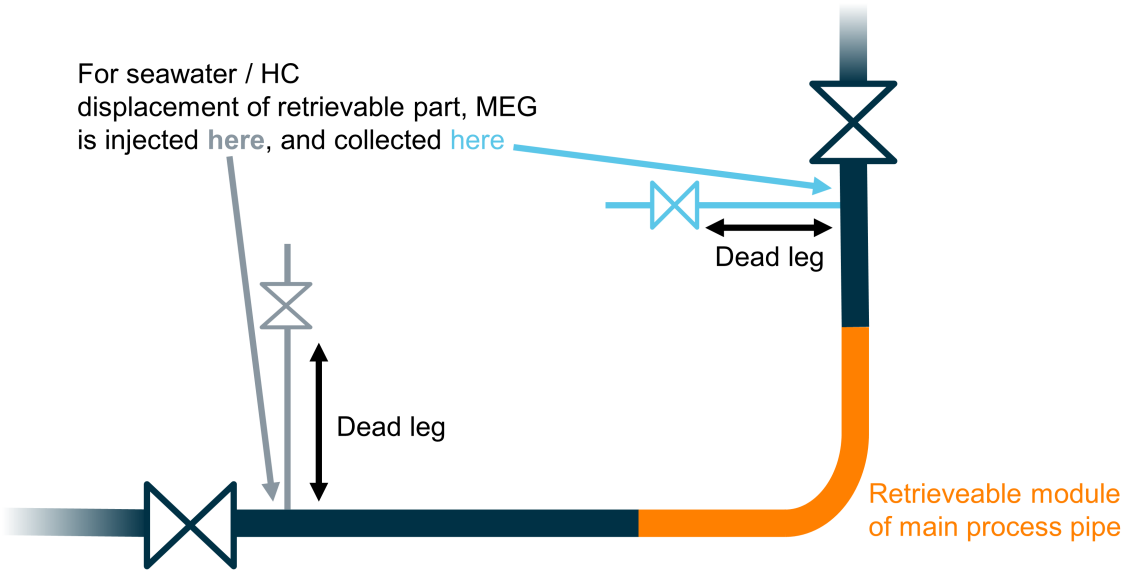

Figure 1.2: Schematic of possible small bore connections to main process pipe.

1.1 Aim

The aim of the project is to simplify the design process of small bore dead legs by providing a document of guidelines and best practices on small bore piping design to be used within subsea production systems. The best practices will be based on thermodynamic CFD-analysis of dead legs representing different piping design categories. Part of the project includes defining the categories, which may be based on pipe bore size, length, general geometry and function. In order to define the piping design categories, inventory of previous designs must first be taken. Part of the project also includes extending a present in-house CFD-method at Aker Solutions for predicting hydrate formation in pipes to handle arbitrary pipe geometries, such as pipe bends.

1.2 Delimitations

The project is limited to investigations within dead legs formed at small bore connections to large bore piping, of which an example is visualized in figure 1.2. Other types of piping which may also be prone to hydrate formation are not considered. For subsea compression systems, the whole station will be considered. In gas production systems the work will be limited to manifolds and christmas trees.

Modelling and simulation of hydrate formation and growth is performed from a practical stand point and is thus limited to predicting the maximum hydrate formation in a pipe design during certain operating conditions. Thus, the underlying chemistry of hydrate formation and the dynamic growth of hydrates will not be explicitly modelled. Furthermore, only steady operating conditions will be investigated. Transient operating conditions such as start up and shutdown will not be considered. Regarding the extent of hydrate formation, the project is limited to considering the risk of plugging of pipes due to hydrate formation. Other effects associated with hydrates within the system will not be considered. Regarding mitigation and avoidance of hydrate formation, the project is limited to considering design practices, such as geometry and insulation of the dead leg. Other methods of hydrate formation mitigation, such as inhibitor injection or heating will not be considered.

1.3 Societal, ethical and ecological aspects

Ensuring the functionality of small bore connections enables gas operators to efficiently remove all HC in adjacent pipe sections when a module is to be retrieved. Thus this work can reduce the risk of involuntarily emission of HC into the surrounding environment during maintenance. Subsea compression systems allows for more efficient extraction of natural gas, effectively decreasing the energy consumption and possibly carbon dioxide emissions associated with the extraction process. As previously mentioned, natural gas offers a readily available energy source at lower carbon dioxide emission rates compared to coal and oil. Even though natural gas is a fossil fuel, it offers a lower emission alternative to countries now relying on coal or oil. An argument can be made for the implementation fossil-free energy, such as solar and wind, in developing economies. However, shortages and inflated cost of energy is a risk in regions heavily reliant on these types of energy sources, as seen at the time of writing in Europe. The middle ground of cutting out the worst emitters, such as coal and oil, by replacing it with natural gas while implementing solar and wind at reasonable scales allows for reliance and a decrease of carbon dioxide emissions of energy sources. In summary, this work has the potential for a positive ecological impact by mitigating local HC emissions, decreasing the energy consumption of natural gas extraction and potentially decreasing the reliance on heavy carbon dioxide emitters such as coal and oil.

Natural gas is a well-performing choice for regulating power in combination with intermittent renewable energy sources as wind or solar power, as gas turbines can be brought on- and offline with short notice. This especially applies for less developed countries with rapidly increasing power demands which cannot afford the cost or technology maturation of new regulating power sources such as hydrogen. Compared to traditional gas production with topside processing, the subsea variant is autonomous to a larger extent rendering it safer for the operators. This work can thus have a positive effect in terms of societal aspects by increasing the reliance of energy supply and making natural gas extraction inherently safer.

Development of subsea gas technology can help increase production and/or prolong the life of gas fields from the North Sea and thus reduce the European dependence on Russian gas. With war raging in Ukraine and Russian gas to be phased out by the EU, the demand for gas from western countries is very large. Securing energy production is an essential task for all countries and the recent events have highlighted problems with the current energy dependency. Reducing

and in time phasing out the dependency on Russian energy is not only a security concern, but an important ethical decision in favour of democracy and peace.

2
Theory

In this chapter a theoretical background regarding subsea production systems, hydrates and heat transfer is given to familiarize the reader with key concepts included in this work.

2.1 Subsea production systems

Subsea production systems can include production control through subsea christmas trees, flow line connections through manifolds, and various subea processing operations. Subsea processing operations include process fluid separation, cooling and boosting through pumps and compressors.

Subsea christmas trees, named after their likeness to a decorated tree, are an arrangement of valves and fittings placed on top of the wellbore. The function of the trees is to control the production flow out of the well, as well as the injection of fluids or gases into the well. Christmas trees can be outfitted with numerous small bore connections, such as chemical injection points. The small bore connection from the main process piping to the valve controlling the chemical injection creates a dead leg if the valve is closed, which could constitute normal operating conditions depending on the function of the chemical injection.

A subsea production manifold is a common subsea structure designed to combine and connect the production from several wells, before onward export to a downstream facility. The manifolds can also be fitted with valves allowing for production from several wells in specific configurations. Much like christmas trees, manifolds are often fitted with chemical injection points or bleed valve connections, which are prone to forming dead legs.

Subsea separation, i.e. separating liquids from gases in the process fluid, can be performed to allow separate boosting of the fluids through compressors and pumps. Together with subsea coolers, separation and compression form the main unit operations of a dry-gas subsea compression system. The compression of the produced gas allows for either prolonged recovery at a given rate or a faster rate of production. Another upside of increasing the pressure of the produced fluids at the seabed is a decrease in pressure drop along the flow lines, meaning the recovery can be performed more efficiently because of the reduction in power necessary to bring the gas ashore [7]. Throughout subsea compression systems, there are small bore piping connections to the main process flow pipes. Typical functions include chemical injection, displacement and drainage lines.

2.2 Natural gas hydrates

Natural gas hydrates are a solid crystalline compound formed in presence of water and smaller guest molecules such as hydrocarbons. The water molecules in contact with the guest molecules form a cage that traps the guest molecule, and these cages in turn can form crystal lattices which constitutes the hydrate [5]. A visualization of a hydrate lattice consisting of methane and water can be seen in figure 2.1. When the cages form crystal lattice structures not all cages must be full, only enough guest molecules to ensure the stability of the lattice structure are needed [5]. Therefore, there is no strict chemical formula for hydrate formation and a hydration number can be implemented to represent the number of moles of water. Hydration numbers are reported to be in the range of 5.5 - 6.5 for a wide range of pressure and temperature [8]. Eq. 2.1 below expresses the formation and dissociation of a methane hydrate from or to gaseous methane and liquid water, where n represents the hydration number.

$$CH_4\ (\mathrm{g}) + nH_2O\ (\mathrm{l}) \Leftrightarrow CH_4 \cdot nH_2O\ (\mathrm{s}) \tag{2.1}$$

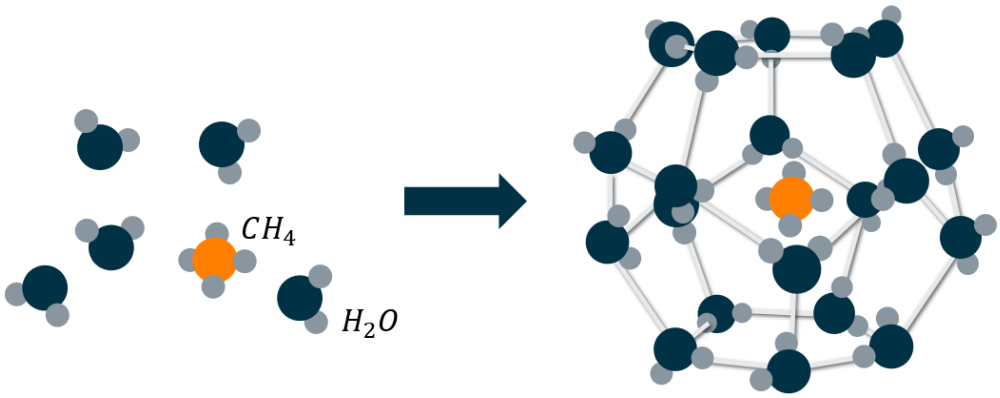

Figure 2.1: Visualization of methane (CH_4) and water (H_2O) forming a hydrate lattice. The lines represent the hydrogen bonds.

From experimental data or thermodynamic computational techniques the hydrate dissociation enthalpy can be determined. The dissociation enthalpy is the energy necessary to break a chemical bond in order to obtain one mole of separate atoms, i.e. the necessary energy to melt one mole of the hydrate . From the dissociation enthalpy a dissociation temperature can be obtained for a given molecular composition at a certain pressure. The hydrate dissociation temperature can also be considered as the hydrate formation temperature, in that below the hydrate dissociation temperature hydrates have the potential to form and grow. In order for the hydrate formation to occur the gas-water system must be maintained below the hydrate dissociation temperature for a sustained amount of time. As stated, the hydrate dissociation temperature is dependent on the molecular composition of the system as well as the pressure. In general an increased pressure and/or reduced temperature will heighten the risk of hydrate formation. figure 1.1 shows how the hydrate dissociation temperature varies with pressure for an imaginary gas/condensate system forming the hydrate curve for that particular system.

In general heavier hydrocarbons form hydrates more readily than methane and so does natural gas compositions encountered in nature [5]. Other impurities such as carbon dioxide, CO_2, and hydrogen sulfide, H_2S, can also elevate the hydrate dissociation temperature. Thus pure methane is the hydrocarbon least prone to forming hydrates.

2.2.1 Hydrate growth in different fluid compositions

Depending on the fluid composition, different models have been suggested to properly capture the nature of hydrate formation, agglomeration and plugging. In an oil dominated system the primary formation of hydrates occurs at the water/oil interface of water droplets dispersed in the oil phase as seen in figure 2.2 [9]. The hydrates form shells around the water droplet and with time agglomerate with other hydrate coated droplets. Eventually these agglomerates may form a plug in the system. Hydrates formed from water dissolved in bulk oil and methane in water is considered negligible.

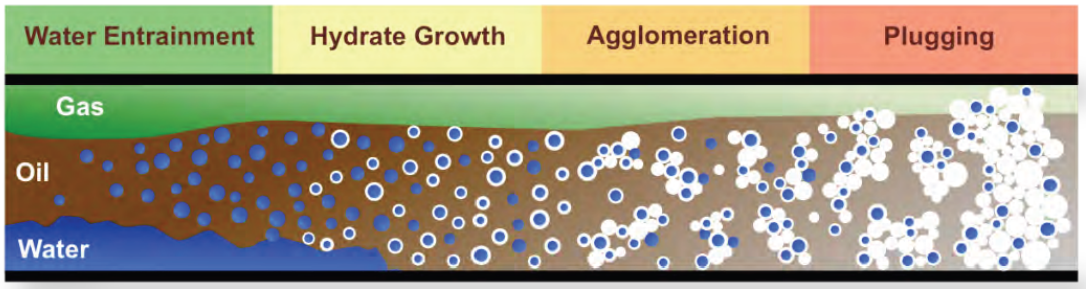

Figure 2.2: Conceptual model for hydrate formation in an oil dominated system, figure courtesy of Koh et al. [10]

For a gas dominated system with small amounts of water and oil a completely different model is suggested. Here hydrate formation occurs at the gas/water interface along the walls and forms an annulus that grows radially towards the pipe center [11]. As the cross-sectional area of the pipe is constrained, the velocity and thereby shear forces increases. This increases the probability for portions of the deposited hydrate to be sloughed from the walls. These free hydrates can deposit further down stream, predominantly in bends or other flow altering parts, forming a plug in that location.

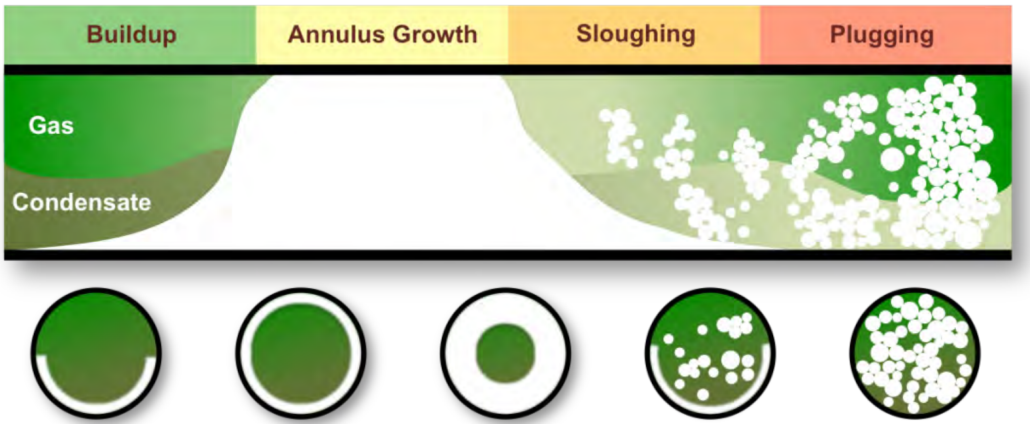

Figure 2.3: Conceptual model for hydrate formation in a gas dominated system, figure courtesy of Koh et al. [10]

2.2.2 Hydrate prevention and inhibition

Several methods can be used to prevent and inhibit hydrate formation and growth, the simplest of which is to ensure all process fluid temperatures are above the hydrate dissociation temperature. This approach is not always viable, as it often requires excessive amounts of insulation and/or active heating of stagnant sections of piping, such as small bore dead legs. If the system temperature can not be kept above the hydrate dissociation temperature chemicals can be injected to delay or inhibit hydrate formation and growth. The most common types of chemicals to inject are thermodynamic inhibitors, such as MEG [7]. Thermodynamic inhibitors shift the hydrate dissociation temperature of the process fluid to lower values, meaning the system can operate at lower temperatures without the risk of hydrate formation. The principle effect of MEG-injection is shown in figure 2.4. MEG can also be used to fill small bore piping in intermittent use, which would otherwise be at risk of plugging by hydrates if filled with water and hydrocarbons. This method is however not always possible to implement since the density of MEG is greater than the density of the produced fluids. Therefore, any MEG-filled piping not connecting at the lower part of the main process piping will be drained of MEG by gravity, and filled with lighter hydrocarbons.

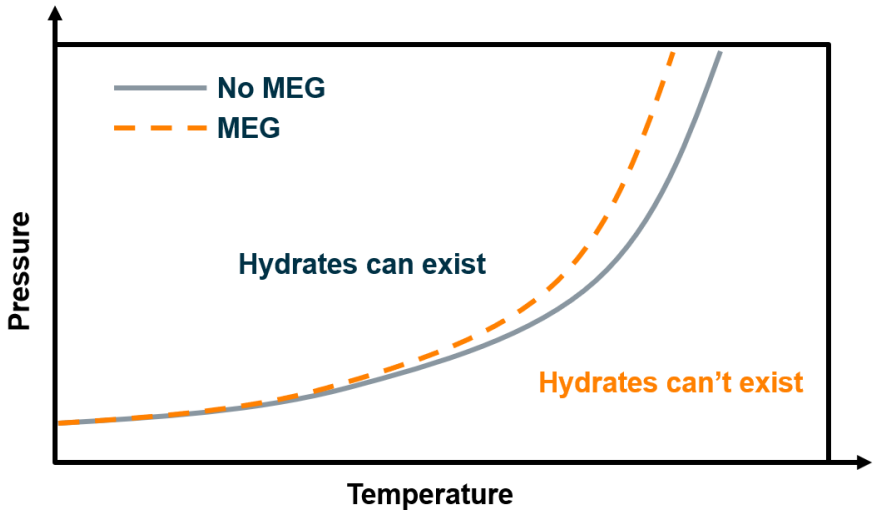

Figure 2.4: Hydrate curve for a typical gas/water mixture, with the effect of MEG-injection.

2.3 Heat transfer in cylindrical pipes

The simplest way to predict hydrate formation is to obtain the local process fluid temperature, either by experiment or by simulation, and compare that to the hydrate dissociation temperature. From a simulation perspective the relevant fundamental physical phenomena is conductive heat transfer through the pipe wall and insulation, and the internal and external convective heat transfer. The combination of these heat transfer mechanisms can be expressed as in Eq. 2.2 [12], where q [W] is the heat transferred, U [W/(m^{2}K)] is the overall heat transfer coefficient (OHTC), A [m^2] is the area over which the heat is transferred and ΔT [K] is the difference between the internal and external temperature.

$$q = UA\Delta T \tag{2.2}$$

It is common to form a sum of thermal resistances, $\sum R_i = 1/(UA)$, where R_i [K/W] represents the thermal resistance of each type of material and/or heat transfer mechanism. A system where Eq. 2.2 can be applied is shown in figure 2.5, a homogeneously formed hydrate is included in the system to highlight the insulation effect of a formed hydrate. For this system five thermal resistances can be expressed, internal and external convective heat transfer as well as three resistances representing the three solid materials. In a cylindrical coordinate system the thermal resistance of the solid materials, taking the insulation in figure 2.5 as an example, can be formed as in Eq. 2.3 [12]. Here, k_{ins} [W/(mK)] is the thermal conductivity of the insulation and L is the length of the pipe.

$$R_{\text{ins}} = \frac{\ln\left(r_4/r_3\right)}{2\pi k_{\text{ins}} L} \tag{2.3}$$

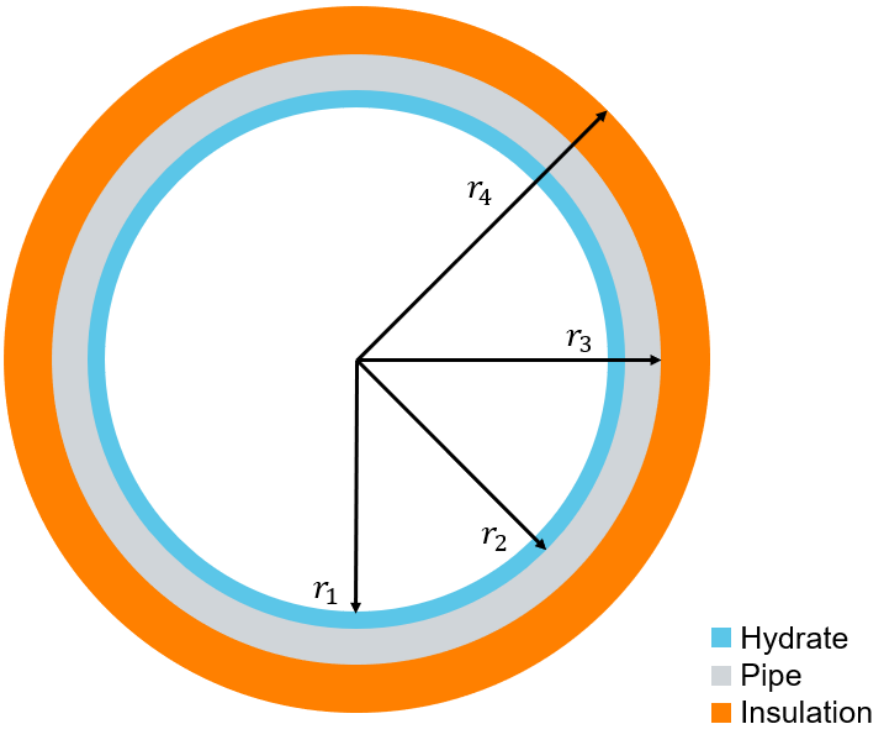

Figure 2.5: Schematic of a pipe with external insulation and a homogeneously formed hydrate on the inside.

Taking the external convection in figure 2.5 as an example, the thermal resistance can be written as in Eq. 2.4. Here, h_{ext} is the external heat transfer coefficient (EHTC). A corresponding expression for the thermal resistance due to internal convection can be formed using the internal heat transfer coefficient (IHTC).

$$R_{\text{ext}} = \frac{1}{h_{\text{ext}} A_{\text{ext}}} \tag{2.4}$$

With the thermal resistances formed and the ambient and center fluid temperatures known as boundary conditions a steady state solution for the temperatures at any location indexed in figure 2.5 can be obtained [12]. For example the temperature T_2 can be obtained as in Eq. 2.5.

$$T_2 = T_a + \frac{R_{\text{int}} + R_{\text{ins}}}{\sum R_i}(T_{\text{center}} - T_a) \tag{2.5}$$

The analytical expressions above explain the fundamental principles of heat transfer relevant to this work. In a thermodynamic CFD simulation expressions like these are not explicitly solved, but rather the ordinary differential equation of energy is solved along with the Navier-Stokes equations. This is a more general approach as it by nature includes three dimensional effects if they exist as well as convective heat transfer based on the flow field and not values of IHTC or EHTC. Still, the fundamental mechanisms of heat transfer explained in this section serve to provide a basis for the physics used in this work.

3
Methodology

In this chapter the methodology for each part of the project is explained. The thesis has two main parts. First methods for predicting hydrate thickness using CFD are evaluated. Secondly design guidelines for small bore dead legs in subsea processing systems are established.

3.1 Hydrate modelling in CFD

Three different methods were tried and evaluated in order to predict hydrate thickness. All methods were based on a pure thermal condition for hydrate formation where they formed as soon as the temperature of the production fluid dropped below the hydrate dissociation temperature. As mentioned, hydrates have a fairly low thermal conductivity and therefore effectively provide insulation between the cold pipe and hot process fluid. At a given hydrate thickness, the temperature at the interface between the hydrate and process fluid would thus be at the hydrate dissociation temperature and no more hydrates would be formed. This process is illustrated in figure 3.1.

In order to validate the methods they were compared with the experimental results obtained by Rao et al. [13]. In their work they conducted a series of experiments measuring the hydrate thickness on a cold steel pipe inside a pressurized gas cylinder called a Jerguson cell. Their experimental set-up is depicted in figure 3.2. The steel pipe was continuously cooled by a coolant line in the center as shown in figure 3.4, however no data was given on the cooling line such as coolant medium, coolant line dimension or volumetric flow. A constant flow (100mL/min) of methane gas saturated with water was supplied into the pressurized gas cylinder. The entire rig was submerged in a water bath.

The EHTC was set to 74 W/m^2K and IHTC to 966 W/m^2K as calculated in [13]. These calculations had some assumptions not necessary to make in the CFD approach where the temperature in the gas could solved rather than approximated by HTC. This led to the IHTC and EHTC being placed on different interfaces in the CFD simulation compared to where they had been calculated in the experiment. These differences are illustrated in figure 3.3.

Five different cases were conducted by Rao et al. with varying pressure, temperature of water bath and cooling line and are summarized in table 3.1.

Figure 3.5 shows the geometry of the entire CFD domain. An orifice was added at the outlet to mitigate backflow effects in the CFD solution due to the low mass flows. Note the white channel

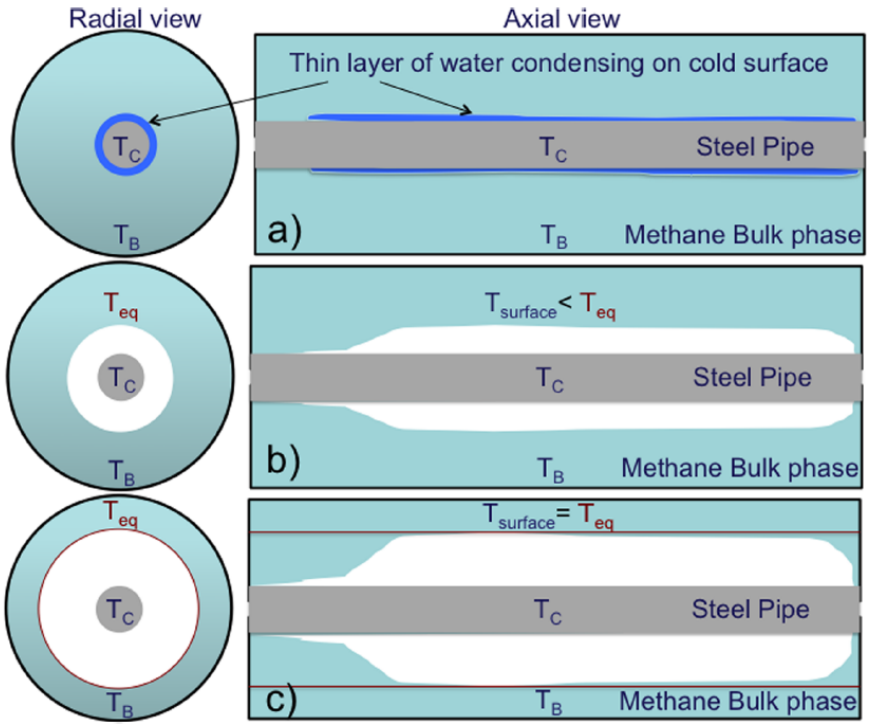

Figure 3.1: Schematic of a) & b) hydrate build up and c) reaching equilibrium thickness. Courtesy of Rao et al. [13]

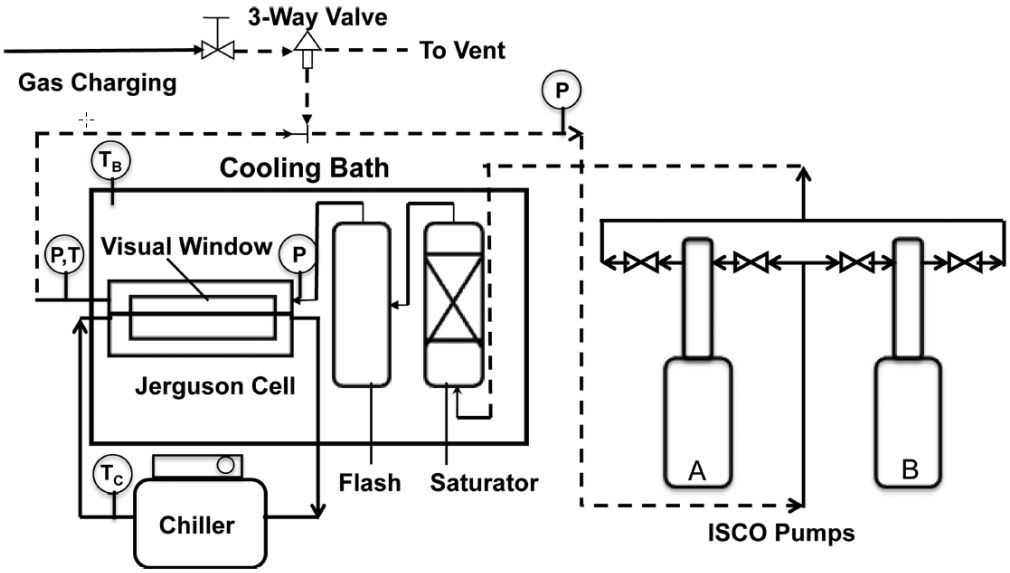

Figure 3.2: Schematic of experimental setup, picture courtesy of Rao et al. [13]

inside the steel pipe representing the cooling line. Figure 3.6 shows the sampling section where the hydrate thickness was measured. Some sections of the steel pipe at the inlet and outlet were neglected to reduce the influence of boundary effects.

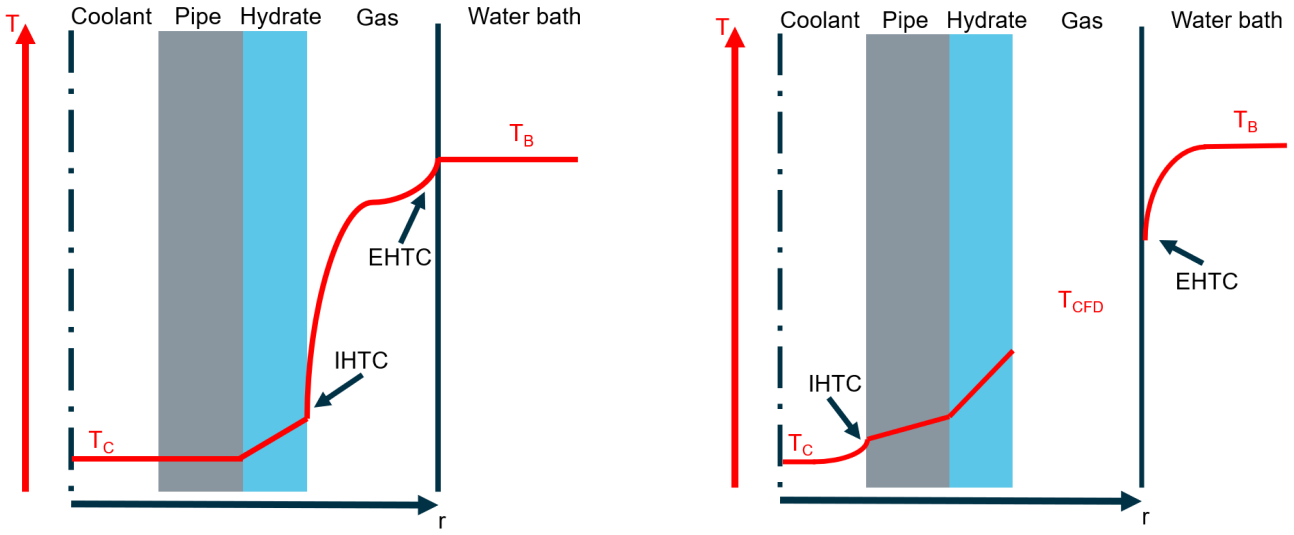

(a) Experimental calculations

(b) CFD

Figure 3.3: Temperature profiles and use of HTC's for experiment and CFD

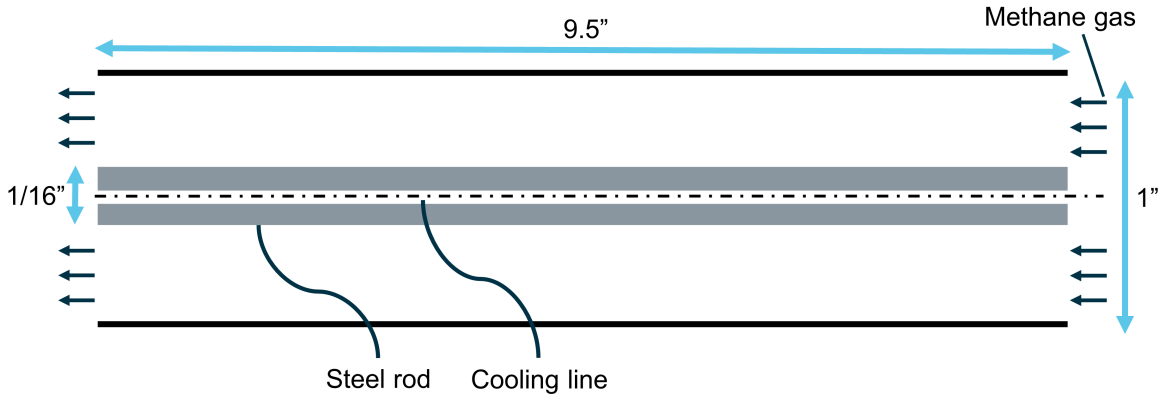

Figure 3.4: Schematic of the Jerguson cell used by Rao et al. [13]

Figure 3.5: Axial view of CFD domain. Fluid region in blue, steel pipe in gold.

Figure 3.6: Zoomed in axial view of CFD domain. Fluid region in blue, steel pipe in gold and measuring section highlighted in purple

3.1.1 Numerical resistance

The first approach tried was with a numerical resistance set at the interface between the process fluid and pipe. If the temperature of the process fluid at the pipe wall was below the hydrate

Table 3.1: Conditions at which experiments by Rao et al. were conducted and the resulting hydrate deposition thicknesses

Case #	Pressure [MPa]	T_B [$°C$]	T_C [$°C$]	T_{HDT} [$°C$]	Final thickness [mm]
1	10.34	22	1	13.3	1.7
2	9.65	22	1	12.6	1.6
3	9.65	25	1	12.6	1.5
4	9.65	22	4	12.6	1.1
5	7.59	22	1	10.4	1.1

dissociation temperature the thermal resistance at the interface would be increased to simulate a growing hydrate layer.

The CFD analysis was performed using steady state conditions based on the operating conditions in the experiment. Two user defined field functions were also used to iteratively find the hydrate thickness (represented here by a thermal numerical resistance) which gave a fluid temperature equal to the hydrate dissociation temperature next to the pipe wall. The numerical resistance, R_{num}, was given as

$$R_{num} = \frac{t_{hyd}}{k_{hyd}} \tag{3.1}$$

where t_{hyd} was the hydrate thickness at that point and k_{hyd} the thermal conductivity of hydrates. In order to get a scalar value to compare with the experimental results, a surface average of hydrate thickness within the sample section depicted in figure 3.5 was made.

3.1.2 Surface wrapping

Another method tried was to isolate regions in the fluid domain with temperatures below the hydrate dissociation temperature. The surface wrapping feature in STAR CCM+ was used on these regions to create and mesh a new solid region within the original fluid domain to represent the hydrates. This new domain was modelled as a solid with appropriate material properties. This approach used a steady state solver and repeated the surface wrapping and meshing after a certain number of iterations until the hydrate thickness had converged.

3.1.3 VOF with Melting-Solidification

The final approach considered was to use the VOF framework and the melting-solidification model. For this approach the simulations were run under transient conditions with a segregated solver. The key premise is to still use a single phase but to let that phase be solidified by stopping flow in cells below a certain temperature. As these simulations were run using a single phase, some compromises were made regarding material properties. Generally each case had temperature dependent methane gas properties accurate for that pressure. The hydrates therefore generally had incorrect material properties with the exception of the thermal conductivity which altered between 0.6 $W/m\,K$ if the cell was solidified and another scalar value (0.04-0.045 $W/m\,K$) for gaseous cells.

In order to reduce the computational cost of a transient solver the velocity field and temperature field were initialized with values from a corresponding steady state case with no hydrate modelling. Also the latent heat of fusion was lowered significantly from around 450 kJ/kg to 0.5 kJ/kg for the same reason.

To accurately capture the solid/gas interface and let the hydrate grow in small portions at a time, adaptive mesh refinement (AMR) was employed with two refinement levels. The magnitude of the gradient of *Relative Solid Volume Fraction* was used as the refinement criteria.

All five cases in table 3.1 were run with the VOF method, however after they were completed, an error in the simulation set-up was noted. The thermal conductivity for the steel pipe was set as ordinary steel ($45\,W/m\,K$) and not stainless steel ($18\,W/m\,K$). This was corrected and two cases (1 and 3) were re-run with corrected thermal conductivity for stainless steel.

3.2 Inventory and categorization

In order to capture representative dead leg designs a number of previously designed systems were analysed, including subsea compression systems, subsea manifolds and christmas trees. This ensured that a wide range of dead leg functions, designs and operating conditions were identified, which in turn made the summarized best practices applicable in a wide range of cases.

To find the dead legs a combination of 3D models as well as piping and instrument diagrams (P&IDs) were used. When found, a number of characteristics of the dead legs were collected in order to categorize them. This included the function and geometry of the dead leg. The categorization of the dead legs began with dividing them into each function and then into the main different designs used for each function as shown in figure 3.7.

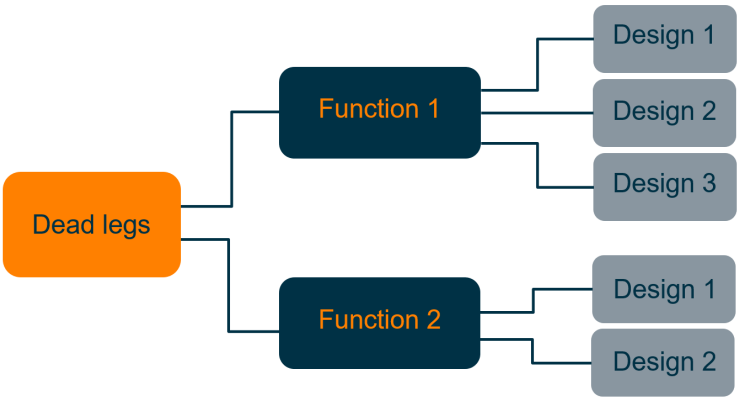

Figure 3.7: Schematic of how the dead legs were categorized

Three main functions for the SB connections were observed:

- MEG injection for hydrate inhibition
- MEG injection for hydrocarbon displacement (HCD)
- HCD lines

Designs for the different categories are presented in section 3.3.2.

3.3 Design evaluation using CFD

To ensure a conservative design that may be used for several different projects and be as generally applicable as possible it is important to use a fluid composition representing a worst case scenario. The chosen composition for the fluid used in this work is seen in table 3.2.

Table 3.2: Gas composition used in CFD simulations

Component	**Molar %**
Methane - CH_4	82.5
Ethane - C_2H_6	10
Propane - C_3H_8	5
Isobutane - C_4H_{10}	2.5

To correct the hydrate curve from pure methane to account for the heavier HC the Trekell-Campbell method was used [5]. Large amounts of the heavier hydrocarbons raised the hydrate curve substantially compared to pure methane as can be seen in figure 3.8. Both curves have logarithmic trendlines fitted to the data points.

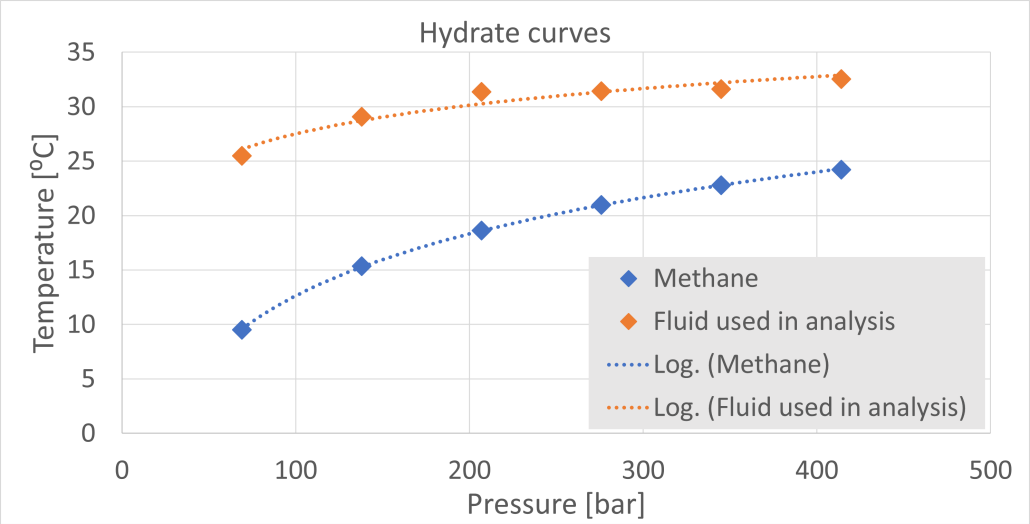

Figure 3.8: Hydrate curve of methane and the resulting curve for fluid composition used in this work

3.3.1 Operating conditions

A number of operating parameters were chosen in order to ensure that the designs are evaluated for a broad range of operating conditions, as well as ensure conservative results. The operating parameters include high and low values for fluid inlet temperature, pressures and velocities as well as hydrate formation temperature (HFT). The values of these operating conditions were

determined with the help of industry standards and experience, which should ensure that the results from simulations, and subsequently the design guidelines, are useful and cover a majority of the operating conditions in future projects. The operating conditions are presented in table 3.3. Note that combinations from both high and low values might be used in the same case for different parameters.

Table 3.3: Operating conditions for thermal analysis in CFD.

	Pressure [MPa]	Fluid inlet temperature [$°C$]	HFT [$°C$]	Inlet Velocity [m/s]
High value	30	30	24	20
Low value	10	10	8.5	10

NORSOK standards state that maximum velocities in gas lines should not exceed the value from the following equation in order to avoid noise and vibrations [14].

$$V = 175 \left(\frac{1}{\rho}\right)^{0.43} \tag{3.2}$$

where V is the maximum velocity in [m/s] and ρ density in [kg/m^3]. Assuming a gas density of 150 kg/m^3 this yields a maximum velocity of roughly 20 m/s. For the lower velocity case, half of this velocity was used.

The high pressure case was set to the maximum discharge pressure possible to achieve with the High-Speed Oil-Free Integrated Motor compressor (HOFIM®) [15] used in current subsea compression projects.

The operating conditions were chosen to represent two conservative cases for studying the temperature field in the dead leg. Both cases operate slightly above their respective hydrate formation temperature and are inhibited with MEG. By evaluating the designs and ensuring that the temperature does not fall below hydrate formation temperature in these operating conditions, it is ensured that the designs operate safely above these temperatures. The small bore dead leg designs that were evaluated with CFD thermal analysis can be seen in figure 3.9.

In a multiphase system that incorporates separation of phases, the properties of any gaseous phase downstream of a separation operation, including HFT, are dictated by the conditions under which separation was performed. This phenomenon is crucial to dead legs that connect to the top part of a main gas production line, as here the gas in the dead leg will effectively be separated from any liquid present in the main line. Following this form of separation, water can condense as the temperature in the dead leg falls, and at some point the MEG concentration in the condensing phase will be below what is necessary to mitigate hydrates from forming. The necessary concentration of MEG to depress HFT by a certain amount can be estimated using Eq. 3.3 [5]. Here, X_R is the concentration of MEG in the aqueous phase in weight percentage, M the molar mass of the inhibitor and ΔT the depression of HFT. K_i is constant equal to 1297.

$$X_R = 100 \frac{M\Delta T}{K_i + M\Delta T} \tag{3.3}$$

The temperature at the point where the concentration of MEG in the condensing aqueous phase matches the concentration according to the equation above is considered as HFT and will therefore vary with varying temperature in the main gas production line.

HFT is determined for one inlet temperature close to ambient temperature (10°C), and one close to HFT without MEG inhibition (30°C). The colder temperature is chosen to represent a conservative case where the operating temperature is much below HFT without MEG inhibition. The hotter case is conservative for all temperatures above 30°C since the difference between operating temperature and HFT will only increase as the operating temperature is increased. If the same conclusions can be made from these two operating temperatures with regards to hydrate formation, the conclusions should also be valid for all operating temperatures above 10°C. The estimated HFTs are presented in table 3.3.

3.3.2 Small bore geometries

Figure 3.9a and 3.9b are examples of small bore connections for HCD lines. They are placed on top of the large bore pipe to ensure all process fluid can be displaced from the piping. The MEG-lock design in figure 3.9c is an example of MEG injection for hydrate inhibition, however it can also be used for HCD lines if placed on top. Finally figure 3.9d shows a v-bend design for MEG injection for HCD. The two MEG injection designs will have MEG remaining in the piping during normal operation and part of the analysis will be to ensure that the MEG does not evaporate or get flushed out. The MEG in these pipes form a "MEG-lock" and ensures that process fluid cannot propagate further down the small bore piping and potentially cause a hydrate plug.

In order to allow for variation in design as well as provide best practices the geometries of the designs were varied in key dimensions. These dimensions include small bore dead leg diameter, small bore dead leg length and bend radius. In addition to this other key factors of the design were changed in order to increase the heat supplied to the stagnant fluid in the dead leg. This change mainly refers to modifying or adding a valve support to the small bore valve. If the valve support is attached to the hot large bore piping, this will create a heat bridge from the hot flowing process fluid to the cold stagnant fluid. The valve support can be seen in figure 3.9b.

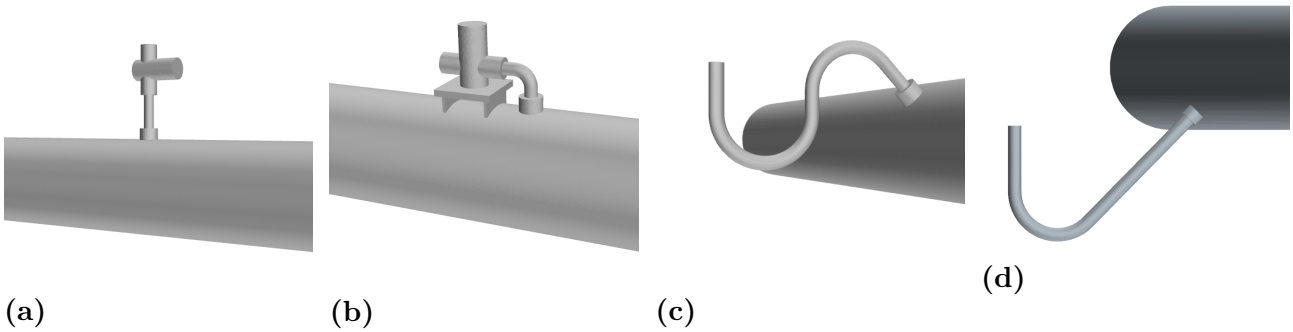

(a) **(b)** **(c)** **(d)**

Figure 3.9: Examples of piping and valve geometry used in CFD thermal analysis.

Small bore dead leg diameters used were 25 and 50mm, two commonly used line sizes in the industry. The small bore dead leg length is varied in an iterative fashion, where the objective

is to find the maximum allowable length of the dead leg before hydrate formation becomes a concern. With the maximum allowable length found in conservative operating conditions, the design can be safely used in more favourable operating conditions.

Other parts of the geometry are kept constant, such as pipe wall thicknesses of the large and small bore piping as well as the insulation thickness. Where insulation is used, it is assumed to be 50mm. For the MEG injection lines the small bore piping will have no insulation in the v-bend case. For the MEG-lock HCD designs, two different insulation arrangements are investigated with regards to evaporation and dilution of MEG.

3.3.3 CFD thermal analysis

The CFD-approach for the thermal analysis of the small bore dead leg designs was to isolate the dead leg on a large bore pipe and simulate it in steady operating conditions. This allows for a simple straight large bore pipe to be used for simulating the main process flow, which has the benefit of cutting down simulation time and complexity. To give an accurate representation of the system in terms of thermal performance, the fluid, piping and insulation were all included and resolved as specific regions in the CFD simulation. These regions are visualized in figure 3.10. In order to capture the heat transfer from the insulation external walls to the surroundings, a conservative EHTC of 1000-2000 [W/(m^{2}K)] was applied and the heat transfer was calculated analytically, similarly to what was shown in section 2.3, together with an ambient temperature of 4°C. When present, the MEG was also included in the CFD simulations. In the thermal analyses the MEG is stagnant in a part of the dead leg, with a single interface to the process fluid as shown in figure 3.11. The MEG was treated as static in order to save the computational time and effort required by a multiphase thermal simulation. This means that the convection of the MEG is neglected, however it is represented by it's relevant properties such as density and thermal conductivity.

Since only steady state operating conditions are considered and the steady state heat balance is sought after, there is no need to resolve the fluid flow and heat transfer in time. This means transient CFD simulations can be avoided, which cuts the simulation time and cost by several orders of magnitude as heat transfer balances can take anywhere from hours to days of real time to reach. However, it is not necessarily true that the fluid flow and heat transfer will find a perfect steady state balance. An example of this could be vortex shedding at pipe bends which will vary in time and thus both the fluid flow and the heat transfer will be affected. To remedy this, the results are averaged over a suitable number of iterations in the steady state solver so that short period fluctuations in heat transfer balance are neutralized. This is also used as a convergence criteria for the solution; when the sliding window temperature field average is no longer changing the simulation can be considered converged.

As mentioned above the fluid flow and heat transfer is resolved in the CFD-simulations with a steady state solver, specifically a segregated solver using the SIMPLE algorithm. The turbulence model used in the thermal CFD-analysis is the elliptic blending (EB) $k-\epsilon$ turbulence model. The reason for choosing this specific turbulence model is associated with resolving natural convection, for which the turbulence model has shown to be robust [16]. The natural

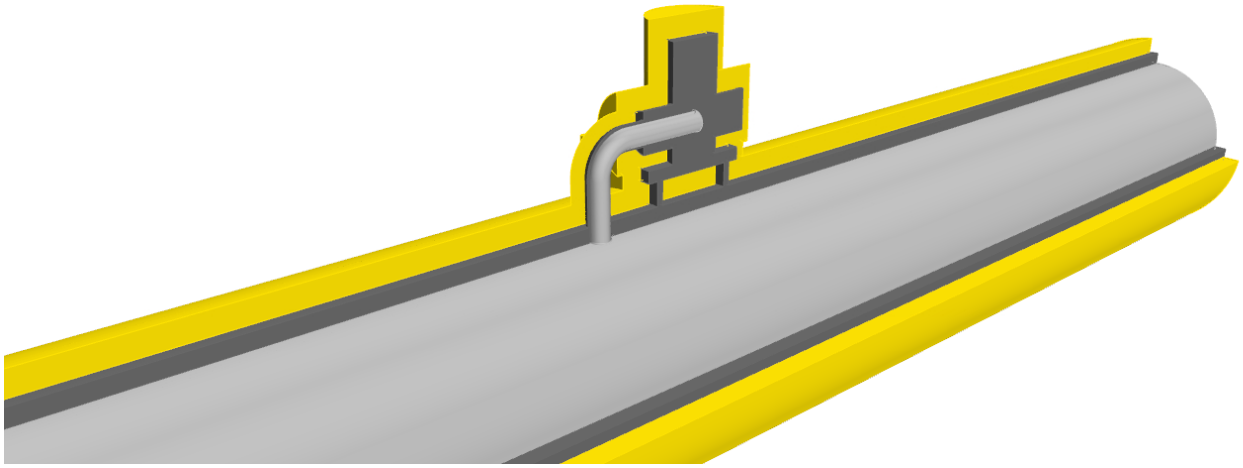

Figure 3.10: Example of the fluid (light grey), piping, valve and valve support (dark grey) and insulation (yellow) regions in the CFD simulations.

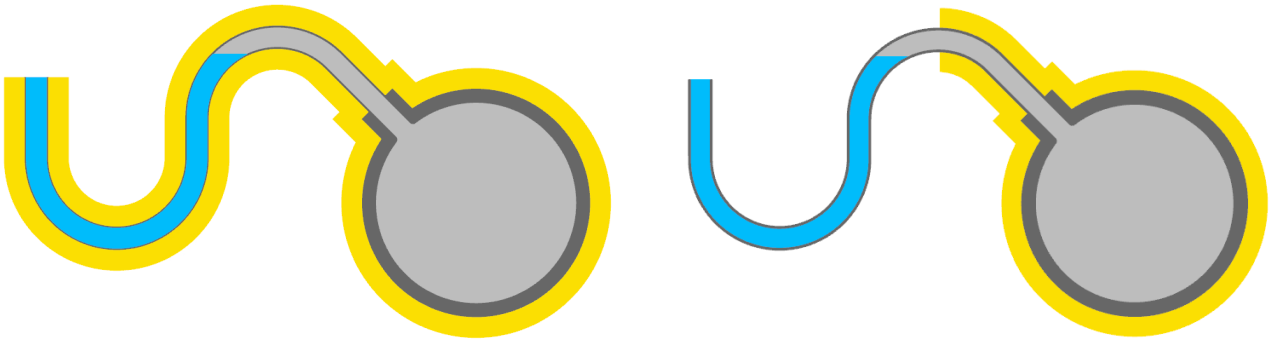

(a) Fully insulated.

(b) Alternative insulation.

Figure 3.11: Visualizations of the fluid (light grey), piping (dark grey), insulation (yellow) and MEG (blue) regions in the CFD simulations.

convection is resolved by implementing a temperature dependent density in the fluid region. Other relevant fluid properties, such as the viscosity, thermal conductivity and specific heat are also temperature dependent. The properties varies according to polynomials in temperature, which are fitted to data supplied from a process simulation software.

3.3.4 V-bend design

Due to the dynamic pressure of fast moving process fluid in the large bore pipes some MEG is expected to be flushed out of the small bore pipe and be replaced by HC. Hence for this design not only a thermal analysis is needed but also a multiphase prediction of where the MEG surface is located in the small bore pipe.

To answer both these questions two simulations were done for each case, the first being a tran-

sient multiphase simulation with the Euler-Euler framework to determine the MEG surface. The gas was modeled as the continuous phase and MEG as the dispersed one. To model the MEG phase the S-gamma particle distribution model was used to model the MEG phase droplet size. A segregated solver was employed to solve the momentum and continuity equations but not the energy equation in order to simplify the simulation. As a consequence of not including temperature in the solution all material properties were set constant. To model the turbulence the SST k-Omega model was used. It combines the accuracy of the standard k-Omega in the boundary layer while using the robustness of the k-Epsilon for the free-stream [17].

Using the results from the multiphase simulation a steady state, single phase simulation was performed to get the temperatures of the process fluid. The simulations were set up similarly to the ones discussed in section 3.3.3. To simplify the simulation the MEG in the SB pipe was modeled as a solid but with correct material properties besides the lack of viscosity. In addition an 80 $^\circ C$ case was run to evaluate how this could effect evaporation of MEG.

4
Results

In this chapter the results are presented. First the results from the hydrate modelling using CFD are presented followed by the results from the design evaluation. The design evaluation is in turn split into two. First the three designs where only a thermal analysis was done are presented and lastly the V-bend design is presented where an additional simulation was performed to determine the location the MEG-surface.

4.1 Hydrate modelling in CFD

In this section the results from the three different hydrate modelling approaches are presented.

4.1.1 Numerical resistance

Two cases were run with this method and both over-predicted the hydrate thickness substantially as seen in table 4.1, which shows the average hydrate thickness around the surface of the steel pipe. Both cases had maximum hydrate thickness equal of that of the distance to the outer pipe wall. This occurred at the bottom of the steel pipe. Thus the pipe was partially plugged at the bottom.

Table 4.1: Comparison between our CFD model with numerical resistance and the experimental results

	Final thickness [mm]	
Case	Exp	CFD
1	1.7	8
5	1.1	5.1

4.1.2 Surface wrapping

The surface wrapping method was never able to run properly. Problems rose during meshing of the newly wrapped "hydrate" region. Cells were self intersecting due to parts of surface wrap being very thin. No case could be run and at a maximum a single iteration was performed.

4.1.3 VOF with Melting-Solidification

The results from using the VOF method are presented in figure 4.1 and table 4.2. Case 1, 2 and 5 all over-predicted the hydrate thickness with 30-40% while case 3 and 4 under-predicted

the hydrate thickness with 10-30%. Case 1, 2 and 5 differed only by the pressure they were conducted in (and thus hydrate equilibrium temperature). Both case 3 and 4 had the same pressure as case 2 but altered water bath temperature and cooling temperature of the steel pipe respectively.

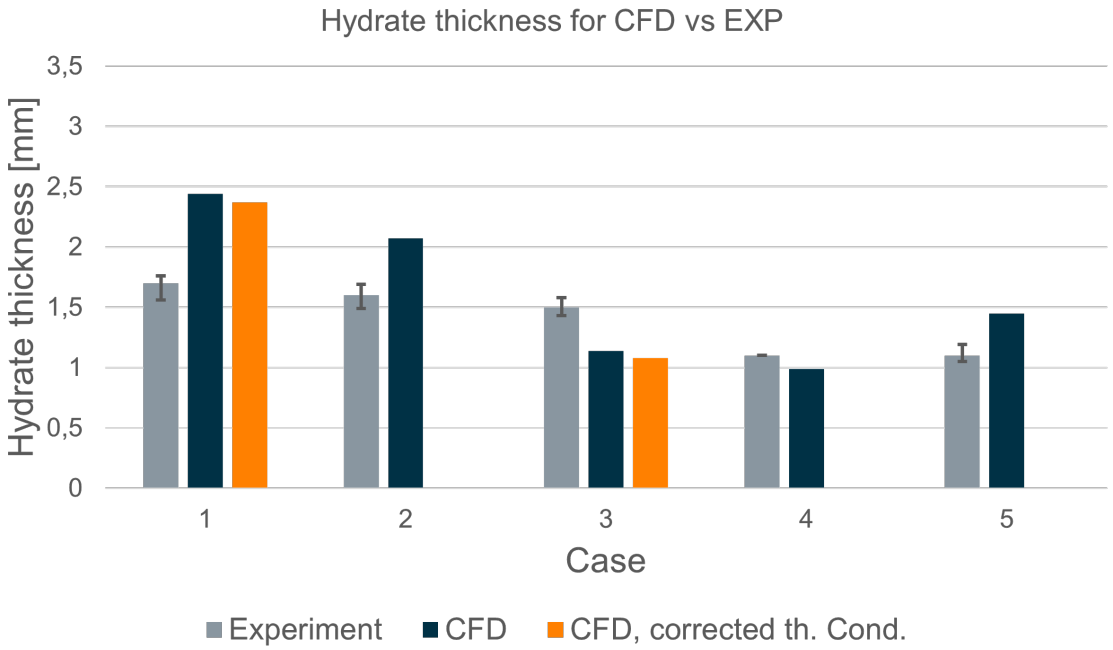

Figure 4.1: Comparison of CFD results with the experimental results obtained by Rao et al. [13]. For case 4 no error margins were presented in the paper but should be of equal magnitude to the other cases.

The two cases ran with a corrected thermal conductivity for the steel pipe (orange bars in figure 4.1) both showed a reduction of the hydrate thickness smaller than 0.1mm. The decrease of thermal conductivity from 45 (ordinary steel) to 18 (stainless steel) $W/m, K$ made no significant impact. Therefor the remaining cases were not repeated with the corrected thermal conductivity.

Table 4.2: Comparison between CFD model and experimental results

	Final thickness [mm]			Difference to exp. [%]
Case	Exp	CFD	CFD corr. th. cond.	
1	1.7	2.44	2.37	44 (39)
2	1.6	2.07		29
3	1.5	1.14	1.08	-24 (-28)
4	1.1	0.99		-10
5	1.1	1.45		32

The hydrate thickness was relatively uniform in the axial direction but varied significantly in

the circumferential direction as seen in figure 4.2 and 4.3.

Figure 4.2: Hydrate distribution in a axial view, hydrates in red, methane gas in blue

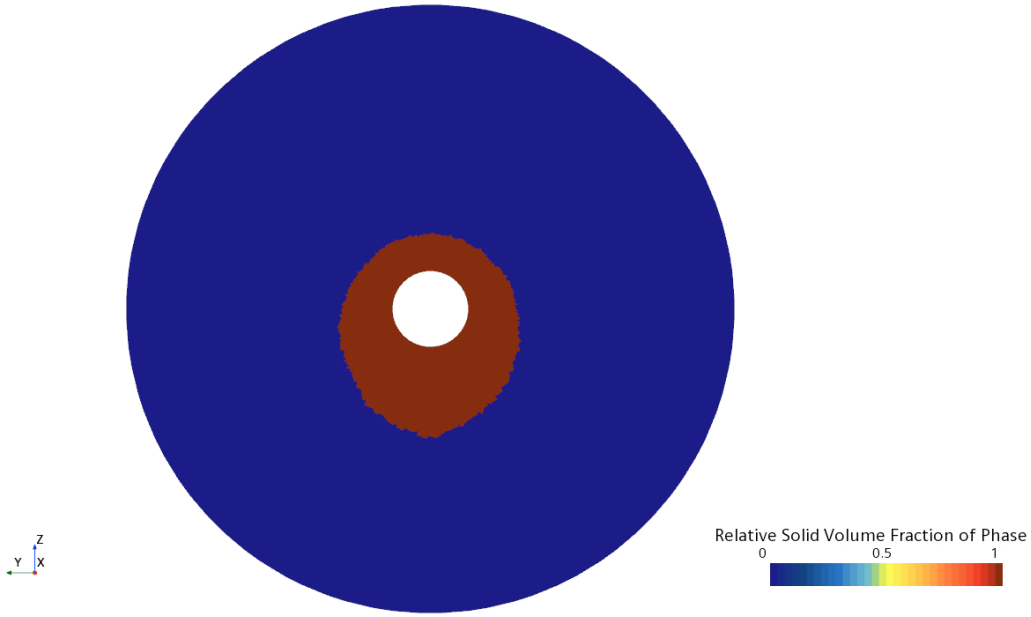

Figure 4.3: Hydrate distribution in a radial view, hydrates in red, methane gas in blue

4.1.3.1 Influence of AMR

The use of AMR enabled the hydrate to grow faster and thicker as seen in figure 4.4. Without AMR the curve flattens out at around 1.1mm. As soon as AMR was turned on, the thickness spiked and rapidly increased to a new plateau of 1.45mm. With 2 refinement levels of AMR, another smaller spike was observed and a thickness of 1.55mm obtained. However the cell count increased rapidly from 0.6 million cells without AMR, to 1.2 million with 1 refinement level and finally 3.2 million with two refinement levels. The use of two refinement levels thus resulted in an increase of 40% compared to no AMR.

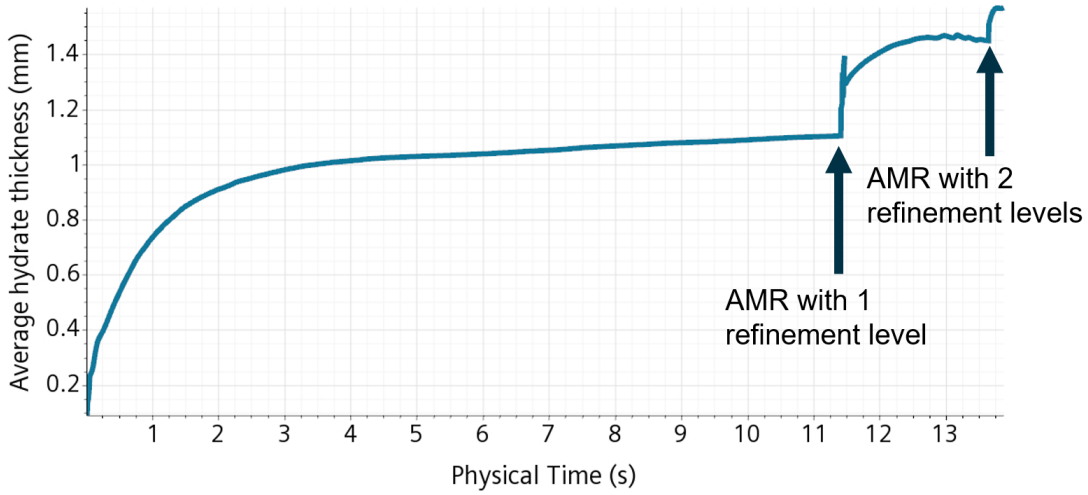

Figure 4.4: Hydrate thickness affected by enabling AMR in two steps

4.2 CFD thermal analysis

In this section the results of the CFD thermal analysis are presented for a number of different designs, namely different designs of hydrocarbon displacement (HCD) lines. Since the majority of the results regard temperature fields in the small bore dead legs, and whether the temperature falls below HFT, the temperature fields are normalized according to Eq. 4.1 in order to clearly show if, and where, the temperature falls below HFT.

$$\bar{T} = \frac{T - T_{\text{HFT}}}{T_{\text{inlet}} - T_{\text{HFT}}} \tag{4.1}$$

The normalization above results in a value of 1 when the temperature is at or above the inlet temperature, and a value of 0 when the temperature is at or below HFT. For the remainder of this chapter, all figures showing a normalized temperature field are normalized according to the equation above.

4.2.1 Vertical valve HCD lines

In figure 4.5 the temperature field in the center of the small bore dead leg is shown in the two operating cases described in section 3.3.1. It is clear from the figure that the maximum allowable length of such a dead leg is shorter than the length of the geometry, since the hydrate formation temperature is reached well before the dead leg ends in the closed valve. Even though the two operating cases have a different temperature difference between inlet temperature and HFT, one can judge from the figure that the maximum dead leg length is similar. This is because the hotter case, with a larger temperature difference to HFT, also has a larger temperature difference to the ambient temperature. Consequently, the case with the higher inlet temperature also cools down faster along the dead leg length. It is beneficial that the two cases show similar maximum dead leg length because the same design guideline can be used for both operating conditions.

In order to investigate the affect of valve placement on the temperature field in the dead leg, the valve is moved closer to the large bore piping. Specifically to the maximum length suggested in

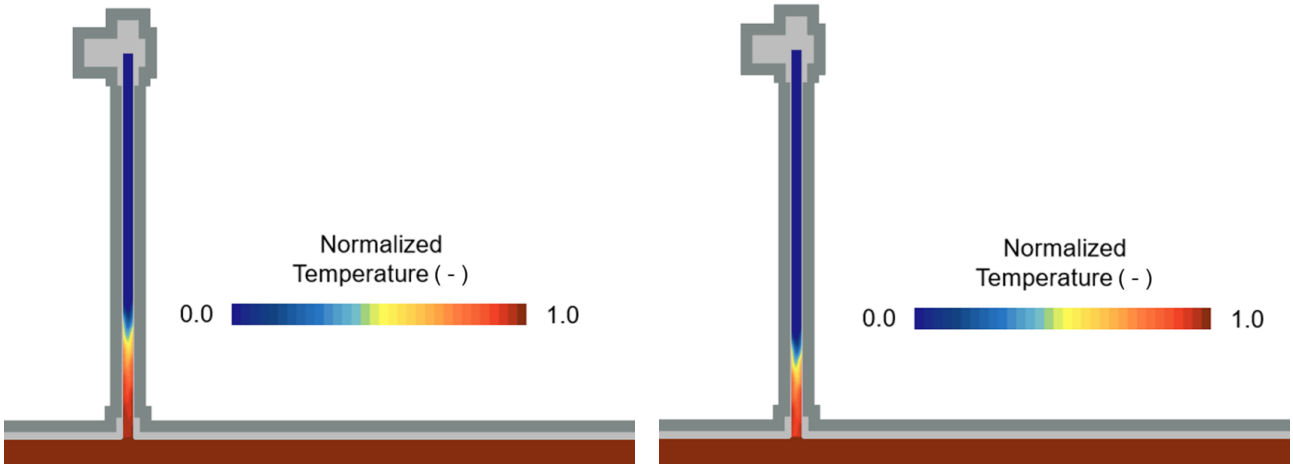

(a) 10°C inlet temperature, 8.5°C HFT. **(b)** 30°C inlet temperature, 24°C HFT.

Figure 4.5: Normalized temperature section in a long, 50mm internal diameter, straight HCD line in two different operating conditions.

figure 4.5. The affect of moving the valve closer to the large bore piping can be seen in figure 4.6. The temperature is slightly lower in the shorter dead leg and is just above HFT at the highest point, at the interface to the valve.

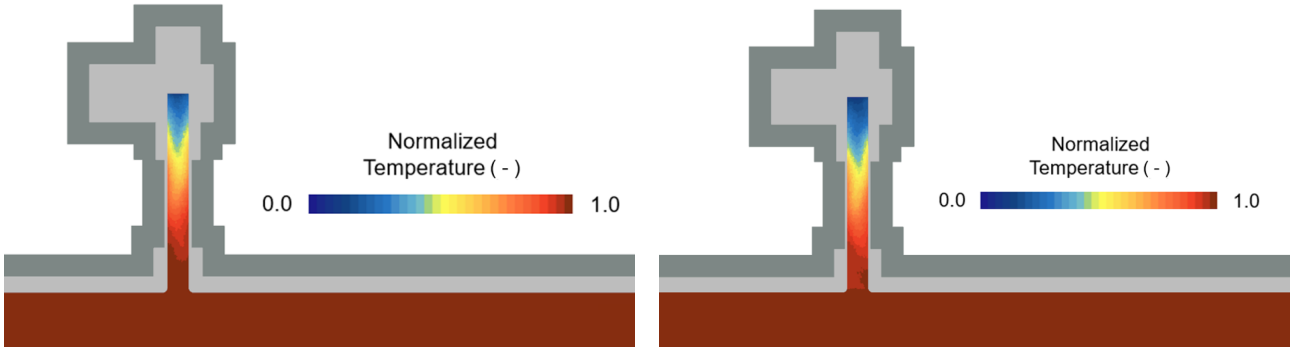

(a) 10°C inlet temperature, 8.5°C HFT. **(b)** 30°C inlet temperature, 24°C HFT.

Figure 4.6: Normalized temperature section in a short, 50mm internal diameter, straight HCD line in two different operating conditions.

In figure 4.7, the flow structure inside a vertical valve HCD line is visualized using the velocity magnitude and directional lines. In the figure, there is division between high and low velocity magnitude. The first region, with a high velocity magnitude, can be considered a primary mixing zone driven by the main process flow detaching and swirling up in to the small bore dead leg. The secondary region with a lower velocity magnitude is mainly driven by natural convection. Comparing these regions to the temperature regions in figure 4.5, one can see a similar division between hot and cold. This indicates that the primary mixing, due to some of the high velocity flow in the main process pipe detaching and colliding with the small bore wall, is an important mechanism for supplying heat to the dead leg and for keeping the temperature above HFT.

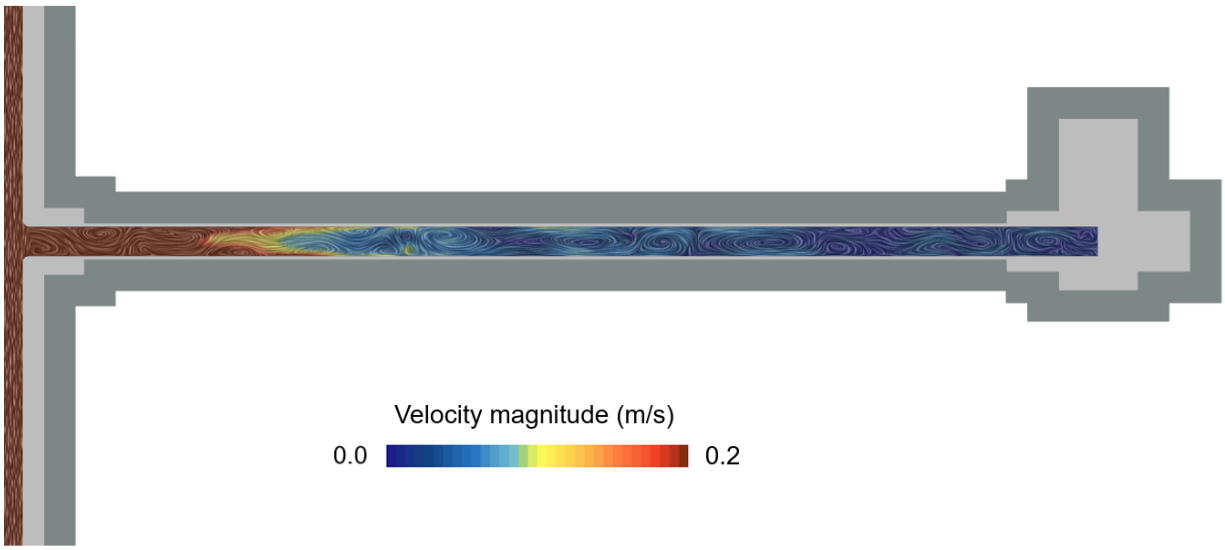

Figure 4.7: Flow visualization in straight, 50mm internal diameter HCD line. Note that the geometry is rotated 90° clockwise.

4.2.2 Horizontal valve HCD lines

In figure 4.8 and 4.9 the temperature field in the center of a horizontal HCD line is shown for two different cases, with and without a valve support. It is clear from the figures that the valve support is improving the thermal performance of the dead leg design by conducting heat from the large bore pipe to the valve. The hot and cold cases are both operating above HFT inside the dead leg with the valve support included. However, without the valve support both cases are operating below HFT in parts of the dead leg. This means that omitting the valve support is not a suitable design choice from a hydrate avoidance stand point.

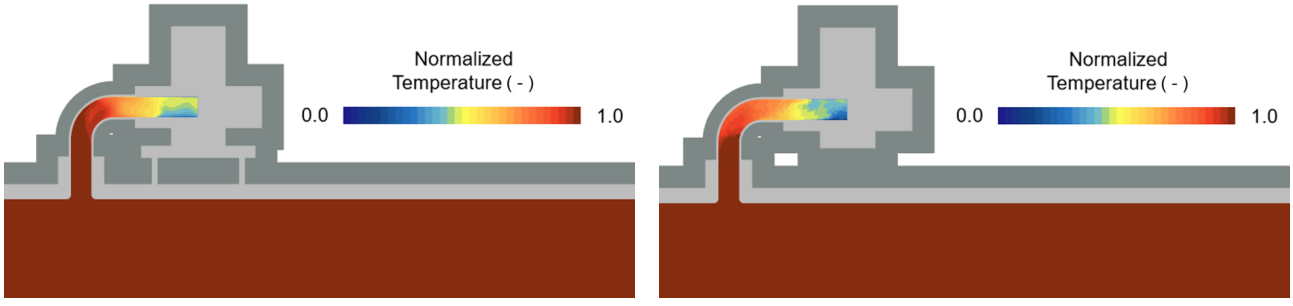

(a) Supported horizontal valve. **(b)** Unsupported horizontal valve.

Figure 4.8: Normalized temperature section in a horizontal valve HCD line, with and without a valve support. 10°C inlet temperature, 8.5°C HFT.

Figure 4.8b and 4.9b show that the hotter operating case has a temperature at or below HFT in a larger part of the dead leg when the valve support is not included. This may seem counter-

intuitive because of the higher inlet temperature and larger temperature difference to HFT. However, as mentioned in the previous section, there is also a higher potential of heat loss in the pipe because of the larger temperature difference between the inlet temperature and the ambient temperature. This is consistent with the results in the previous section, where the colder case is operating above HFT in a slightly larger part of the dead leg. However, in the horizontal valve dead leg design the difference between the two operating conditions is more clear, especially without the valve support included.

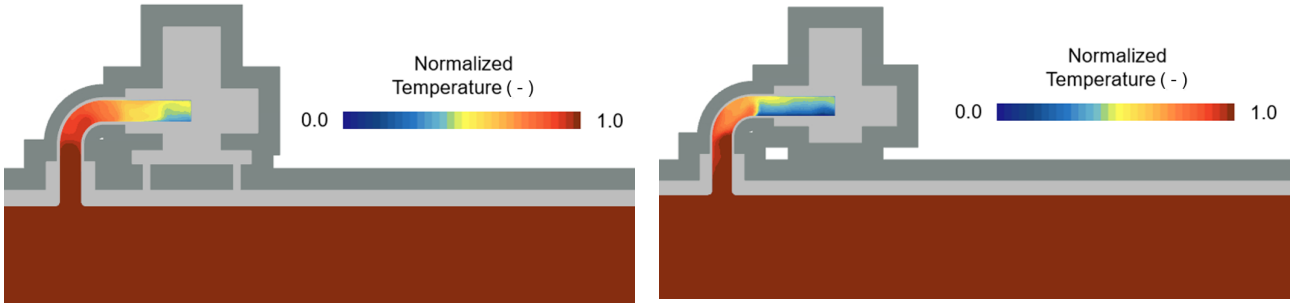

(a) Supported horizontal valve.

(b) Unsupported horizontal valve.

Figure 4.9: Normalized temperature section in a horizontal valve HCD line, with and without a valve support. 30°C inlet temperature, 24°C HFT.

In figure 4.10 the normalized surface temperature on the piping and the valve is shown, where the plates making up the valve support are heated up by the large bore pipe. In turn, the valve support is heating up the valve which supplies heat to the fluid inside the dead leg. The relatively high thermal conductivity of steel combined with the co-insulation of parts is improving the thermal performance of the design by supplying heat from two ends. The valve needs to be supported because of other constraints not under consideration and therefore designing it to improve the thermal performance is an added benefit.

4.2.3 MEG-lock HCD lines

When the normally closed valve on the HCD line can not be placed near the large bore pipe, such as in the designs shown in previous sections, it is common to design the small bore piping in a matter that creates a MEG-lock or trap. An example of such a lock is shown in figure 4.11. The idea is that the design creates a MEG-lock which restricts the gas from migrating further up the dead leg, keeping the majority of the dead leg safe from hydrate formation. The shorter part of the dead leg that is filled with process fluid should however still be kept above HFT in order to prevent hydrate growth.

As can be seen in figure 4.11, the 50mm internal diameter dead legs are operating above HFT in the part of the dead leg which is filled with process fluid. This means that hydrate formation in this part of the dead leg is avoided. The designs investigated are also conservative in the sense that they can be shortened by reducing the bend radius as well as the straight piece of piping connecting to the large bore pipe, meaning there is room for increasing the minimum temperature in the gas part of the dead leg by shortening it. Shortening the dead leg effectively

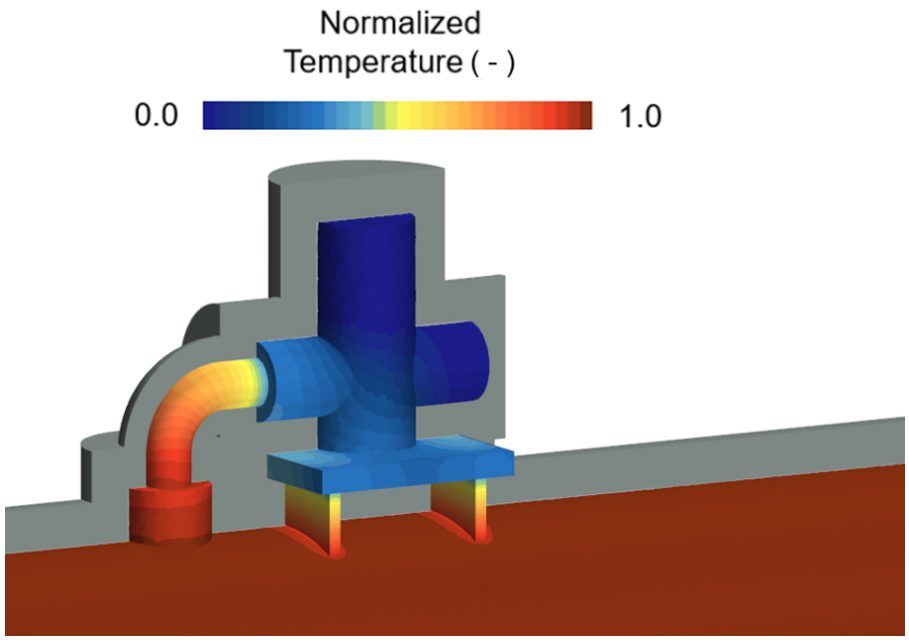

Figure 4.10: Normalized surface temperature visualized on piping and valve.

places a larger portion of it inside the primary mixing zone close to the large bore pipe, which is beneficial in terms of thermal performance.

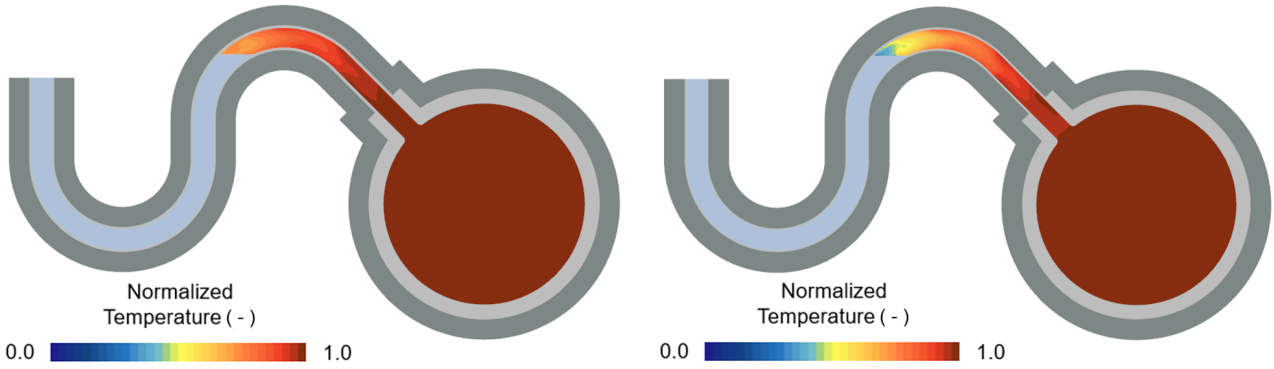

(a) 10°C inlet temperature, 8.5°C HFT.

(b) 30°C inlet temperature, 24°C HFT.

Figure 4.11: Normalized temperature section in a MEG-lock HCD line, 50mm internal diameter.

In figure 4.12 temperature sections from two smaller internal diameter MEG-lock HCD lines are shown. The two designs in the figure are simulated at the same operating conditions, however the design in figure 4.12b has a smaller bend radius. The design in figure 4.12a has the same bend radius as the designs shown previously. Both of the smaller internal diameter designs have a shorter straight section of piping connecting to the large bore pipe. Comparing the figures clearly shows that the longer bend radius design creates a too long dead leg for the process fluid to operate above HFT. Even though the length of the straight section of small bore piping connecting to the large bore pipe is half the length compared to 50mm internal diameter design the long bend radius creates a comparably long dead leg. The reason for halving this section of

small bore piping is to keep the dead leg length divided by internal diameter, L/D, constant. This will be expanded on in section 4.2.4. Clearly only halving the straight section of the small bore dead leg was not sufficient, and so the bend radius was halved as well. From figure 4.12b, it is clear that the process fluid operates above HFT. Comparing figure 4.11 and 4.12 show that more than absolute lengths of dead legs needs to be considered when evaluating the thermal performance. It should also be noted that tight clearances between insulation external surfaces, such as in figure 4.12b, should be avoided since the application of insulation may become troublesome.

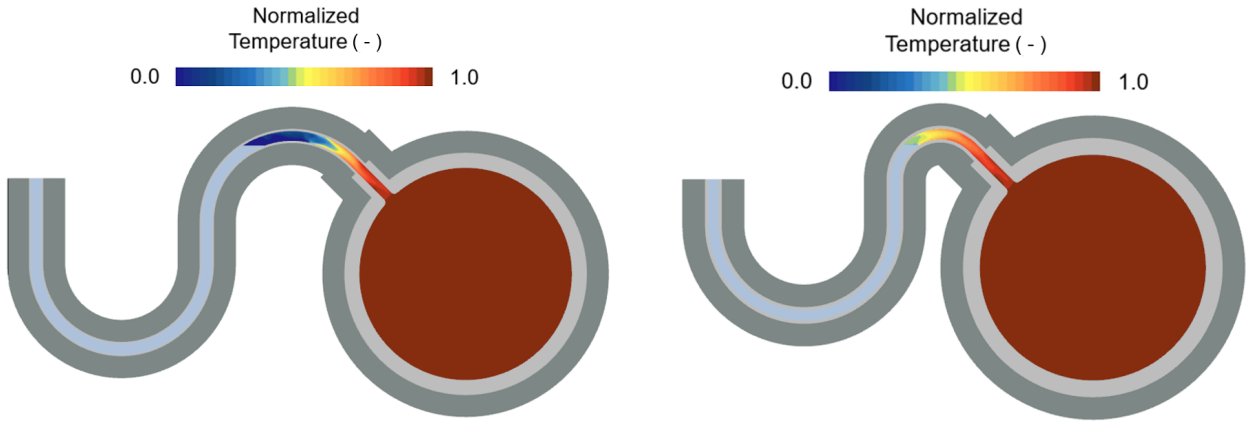

(a) Larger bend radius.

(b) Smaller bend radius.

Figure 4.12: Normalized temperature section in MEG-lock HCD lines, 25mm internal diameter. 30°C inlet temperature, 24°C HFT.

In the MEG-lock design, there is a risk of evaporating and/or diluting the stagnant MEG with condensing water over time. The remedy to this is generally to not have too hot process fluid at the MEG interface. Colder temperatures slow down the process of evaporation. As for condensation, the idea is that it will occur in the straight part of the dead leg connecting to the large bore pipe, allowing it to drip back into the main process pipe as opposed to diluting the MEG. This is contradicting the remedy for hydrate formation, i.e. keeping the process fluid hot. General recommendations for a broad range of operating cases become more complex when setting both an upper and lower limit on the temperature range. The problem of evaporation and condensation adds an upper limit to the temperature range which is deemed suitable. In order to show a possible design change and it's impact, the MEG-lock design insulation is altered so that it ends at the high point of the MEG-lock, as seen in figure 4.13. The same results are shown, but with two different temperature scales, in figure 4.13 to highlight the two contradicting issues. figure 4.13a shows that decreasing the amount of insulation helps with evaporation and condensation. Since the process fluid temperature at the MEG interface is lower less condensation will occur. More of the temperature decrease occurs in the straight part of the dead leg, meaning more condensate should drip back down into the main process pipe. However, figure 4.13b shows that the process fluid is at or below HFT in a large part of the dead leg bend, meaning hydrate formation is a risk.

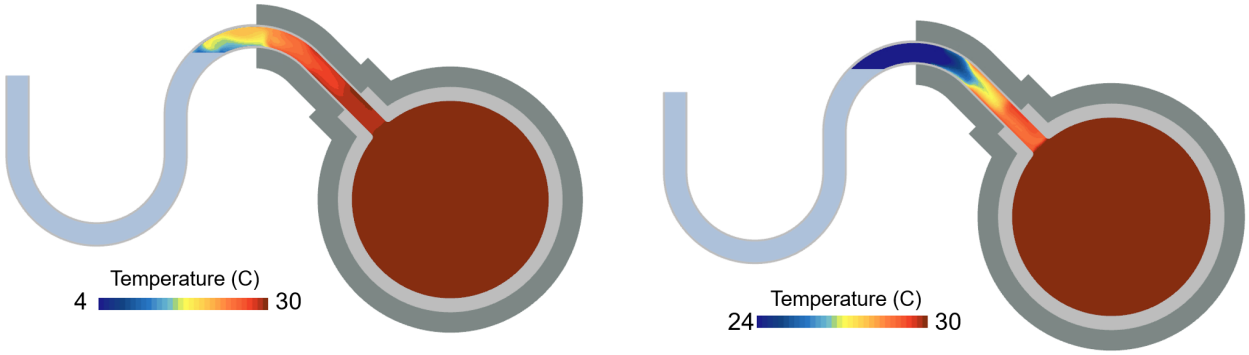

(a) Lower limit of scale set to ambient temperature.

(b) Lower limit of scale set to HFT.

Figure 4.13: Temperature section in a MEG-lock HCD line, not fully insulated. 30°C inlet temperature, 24°C HFT.

4.2.4 Normalization of temperature profile

To give a more detailed insight into the maximum allowable length of a dead leg, the temperature profiles from different cases in a straight, top connecting dead leg, as shown in figure 4.5, are normalized and compared. The temperature is normalized according to Eq. 4.2, and the dead leg length is normalized according to Eq. 4.3, where D is the internal diameter of the dead leg and z is the vertical coordinate in the dead leg. The normalized temperature is a form of temperature potential between the high temperature of the main process fluid flow and the low ambient temperature.

$$\bar{T} = \frac{T - T_{\text{amb}}}{T_{\text{inlet}} - T_{\text{amb}}} \tag{4.2}$$

$$\bar{z} = \frac{z}{D} \tag{4.3}$$

The purpose of this post processing is to investigate if the normalized temperature profiles are similar in straight small bore dead legs for different small bore internal diameters as well as operating temperatures. This helps give a better understanding of the temperature profile in off-design operating conditions, such as different process fluid temperatures. In figure 4.14, four cases are compared by their normalized temperature profiles. The cases consists of two small bore internal diameters, 25 and 50mm, which are simulated at one low and one high process fluid temperature each and otherwise identical operating conditions. As can be seen in the graph, the normalized temperature profiles all follow a similar trend, with a larger decrease in temperature within 10-20 internal diameters and a slower decrease in the remaining part of the dead leg. The first, primary, zone of temperature loss can be described as decreasing proportional to the square of the internal diameter, i.e. $\bar{T} \propto -\bar{z}^2$. And the secondary zone of temperature loss can be described as being decreasing linearly with the internal diameter, i.e. $\bar{T} \propto -\bar{z}$.

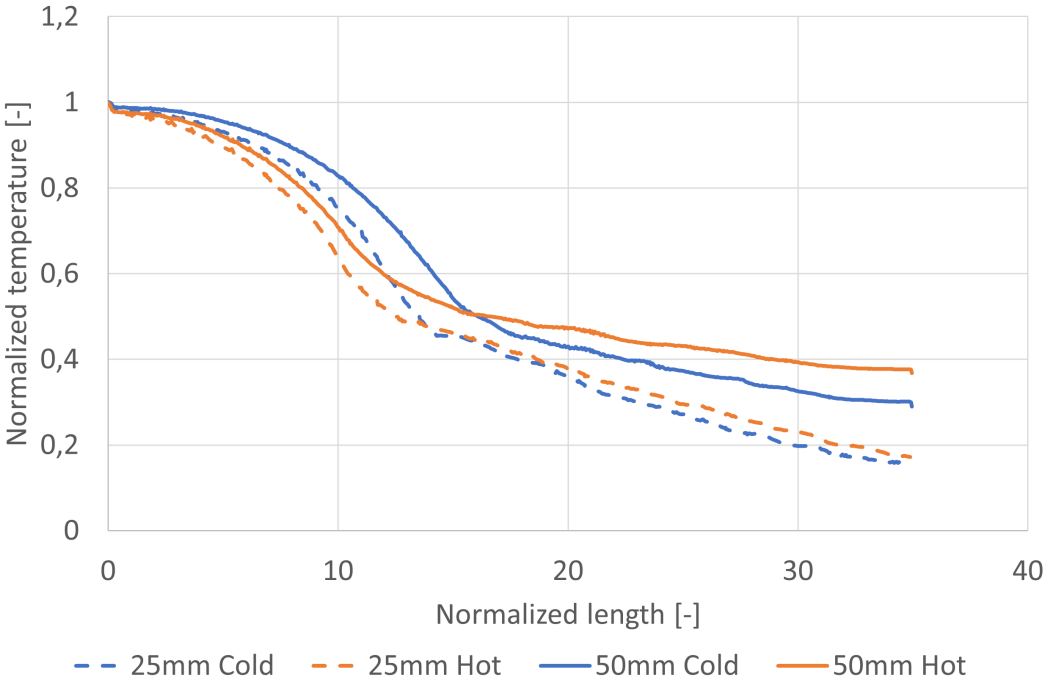

Figure 4.14: Normalized temperature profile in dead leg from four different cases.

As mentioned above the normalized temperature profiles in figure 4.14 are similar, however there is a stronger correlation between the profiles that have identical small bore internal diameter but different operating temperatures. The weakest correlation is between the cases that have different internal diameter and different operating temperatures.

4.3 V-bend

In this section first the results from the multiphase simulation to determine the amount of MEG flushed out is presented. Later, the thermal results evaluating additional displacement of MEG due to evaporation are presented.

4.3.1 Determining MEG level

To measure the amount of MEG flushed out of the SB pipe an isosurface was monitored and set at the interface of the two phases. The MEG surface was found to be located 2-5 inner diameters (ID) down in the small bore pipes in all cases. These results were true for both 50 and 25mm diameter small bore lines. As an example of this, figure 4.15 shows two identical cases with the exception of the small bore pipe diameter, where the difference between the two normalized results is 4.5%.

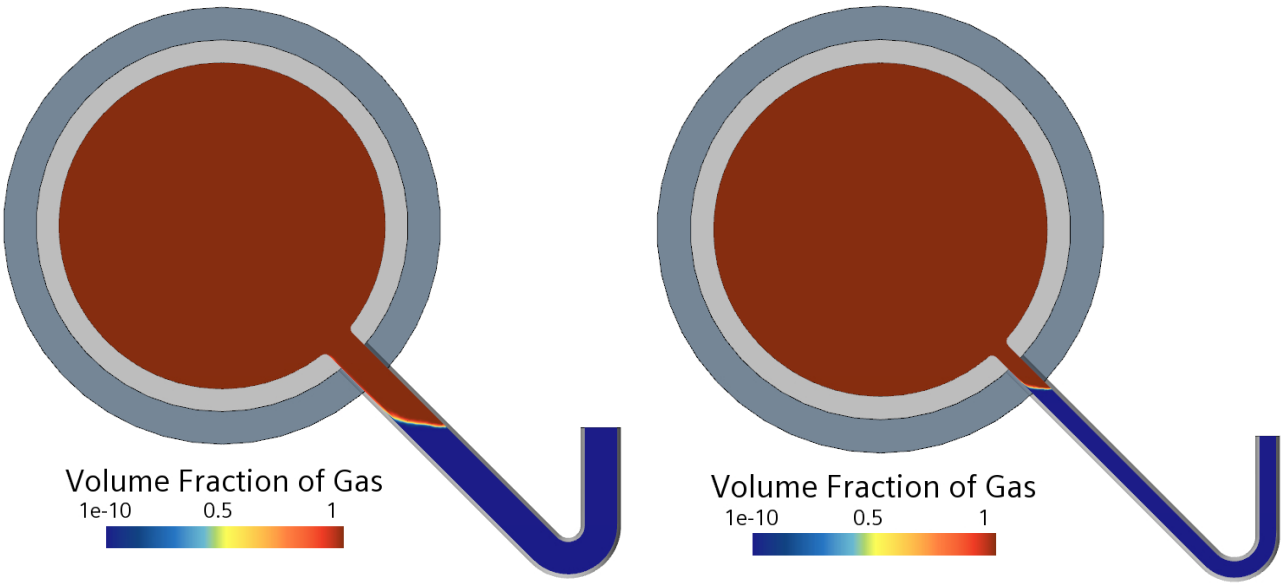

(a) 50mm diameter small bore pipe, MEG surface located 3.6 ID down in SB pipe.

(b) 25mm diameter small bore pipe, MEG surface located 3.48 ID down in SB pipe.

Figure 4.15: Radial view with volume fraction of each phase for two SB sizes in otherwise identical cases. Blue is MEG, red is process fluid. Pipe and insulation (two shades of grey) was not included in this simulation and is included only to give the reader some references to scale.

The higher pressure (300 bar) and velocity (20m/s) cases represented the upper part of the interval while lower pressure and velocity resulted in the lower part of the interval as seen in figure 4.16a. Figure 4.15b shows that inlet temperature has a smaller influence on MEG level in the dead leg.

Plotting the amount of MEG flushed out against the dynamic pressure in the large bore pipe as seen figure 4.17 gives an clear indication that more MEG is flushed out when higher dynamic pressures are present. A logarithmic trendline is fitted to the data and its associated equation

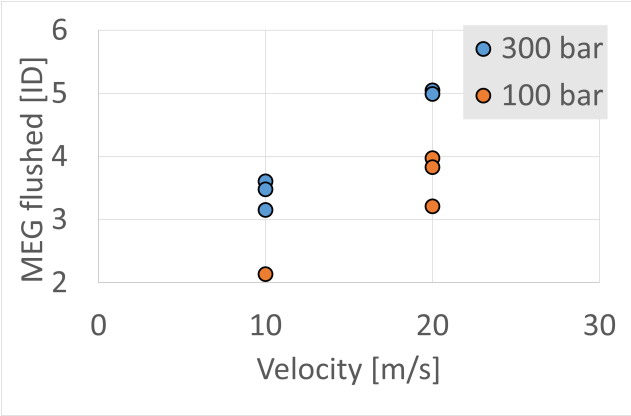

(a) Grouped by pressure and velocity

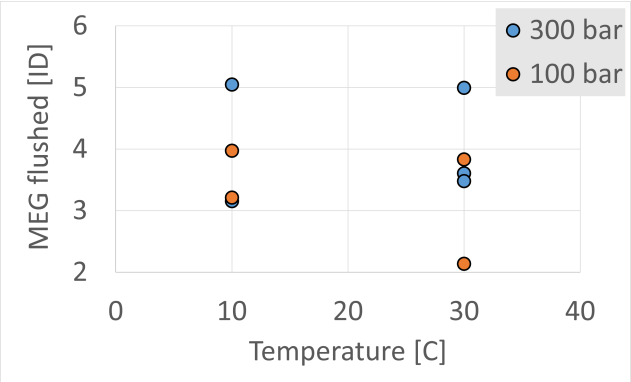

(b) Grouped by pressure and temperature

Figure 4.16: Amount of MEG flushed out of small bore pipe normalized with inner diameter.

can be seen in the figure.

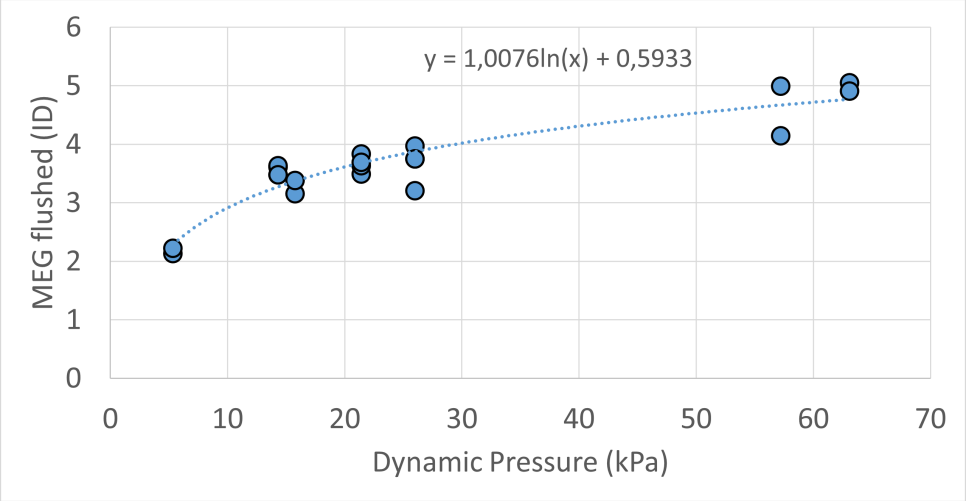

Figure 4.17: MEG flushed as a function of dynamic pressure

To ensure the robustness of the simulation a number of variations of the set-up were run. One case was run with MEG initialized in the lower 1/3 of the large bore (including the small bore) pipe instead of only in the small bore pipe as seen in figure 4.18. Figure 4.19 shows the MEG surface settling on the same height in both cases. Other variations with small bore pipes only a bit longer than where the MEG surface was located, and with a shorter, more complex large bore inlet pipe were also simulated. None of these variations resulted in significant differences compared to the original cases.

4.3.2 Thermal analysis of the resulting deadleg

When normalized temperatures are used in this section they are normalized with respect to inlet temperature and ambient temperature as stated in Eq. 4.2.

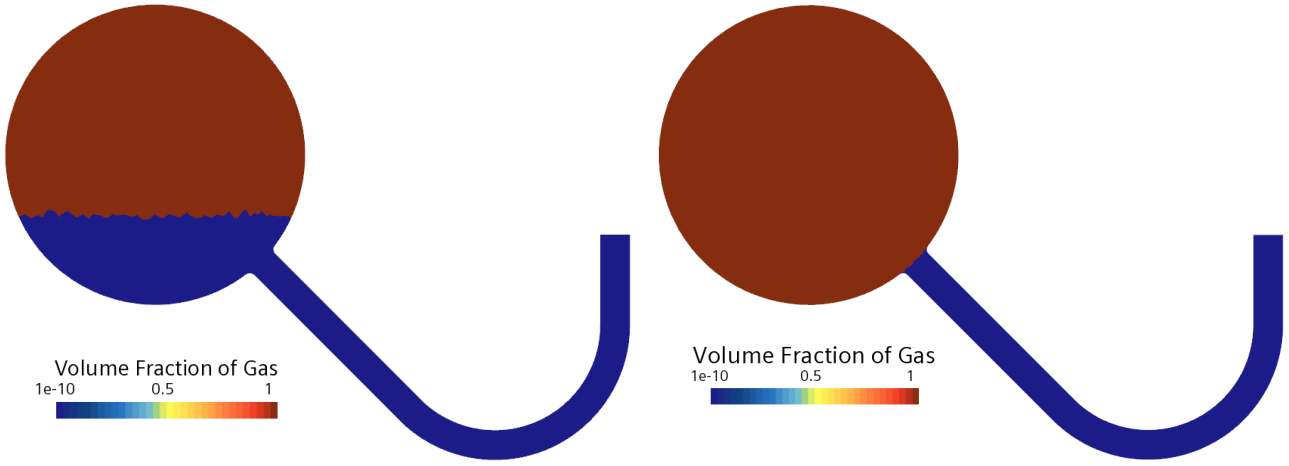

(a) MEG in the lower 1/3rd of the domain **(b)** MEG as initialized in standard cases

Figure 4.18: Initialization of MEG in the domain

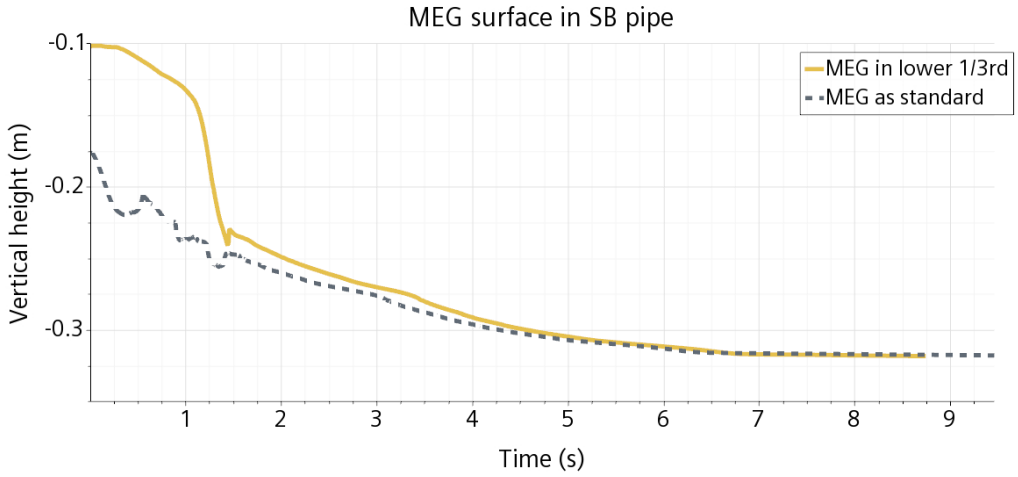

Figure 4.19: Vertical height of MEG surface for different initializations of MEG

After determining how much MEG would be flushed out, the next step was to determine the length of deadleg needed to reduce the effect of evaporation. Figure 4.20 shows the temperature along the small bore dead leg in the axial direction for a number of cases. At the end of these 17 ID long deadlegs all cases are close to ambient temperature.

In figure 4.21 two different amounts of MEG left in the dead leg for the same operating condition are shown. For the 17 ID case the MEG surface is close to ambient temperature. The shorter 8 ID case have temperatures around 40° C at the interface.

Comparing the axial temperature in the small bore pipe for both the longer (17 ID) and shorter (8 ID) case with the same operating condition it can be seen that the curves don't match. Figure 4.22 shows that the shorter case results in a higher temperature than the corresponding location for the longer case.

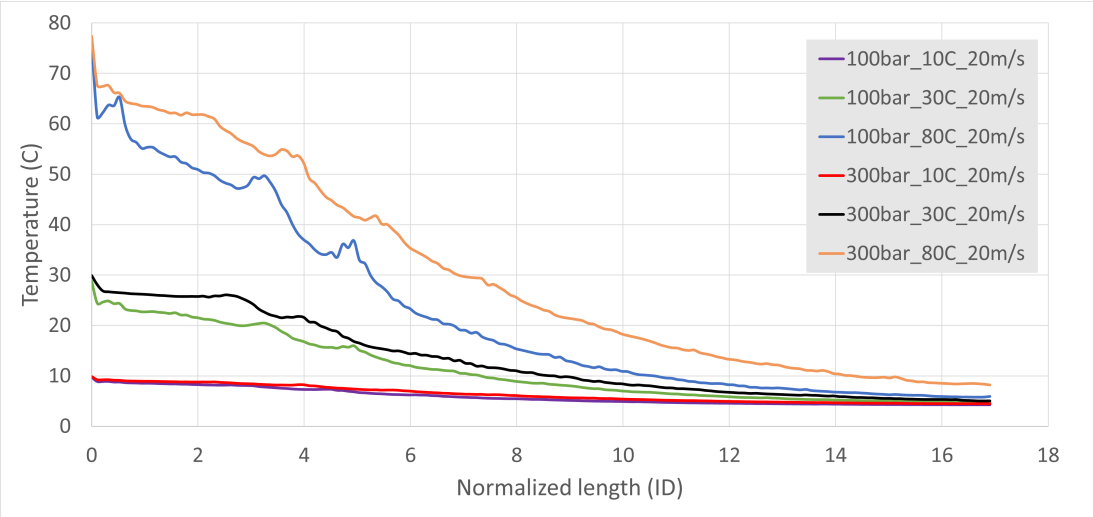

Figure 4.20: Temperature along the axial direction in small bore deadlegs

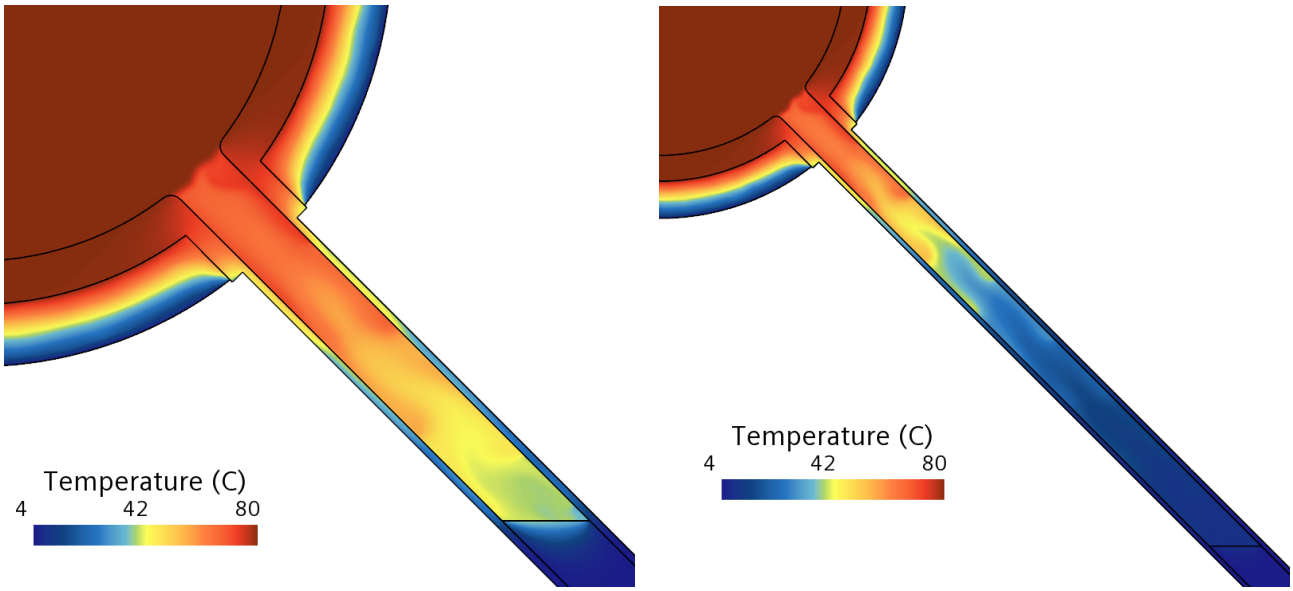

(a) 8 ID down to MEG surface **(b)** 17 ID down to MEG surface

Figure 4.21: Temperature in the deadleg for different amounts of MEG. The black contour lines shows interfaces between different materials.

Regarding geometric similarity two different operating conditions were run with both a 50 and 25mm small bore diameter. The resulting normalized temperatures can be seen in figure 4.23. Both diameters shows good agreement along the entire curve.

From the results it can also be concluded that higher pressure and/or velocity results in a slower cooling of the dead leg. Figures examining this can be found in Appendix A.

Finally, in figure 4.24 a comparison between an insulated and uninsulated small bore pipe can be seen. The uninsulated case is significantly colder.

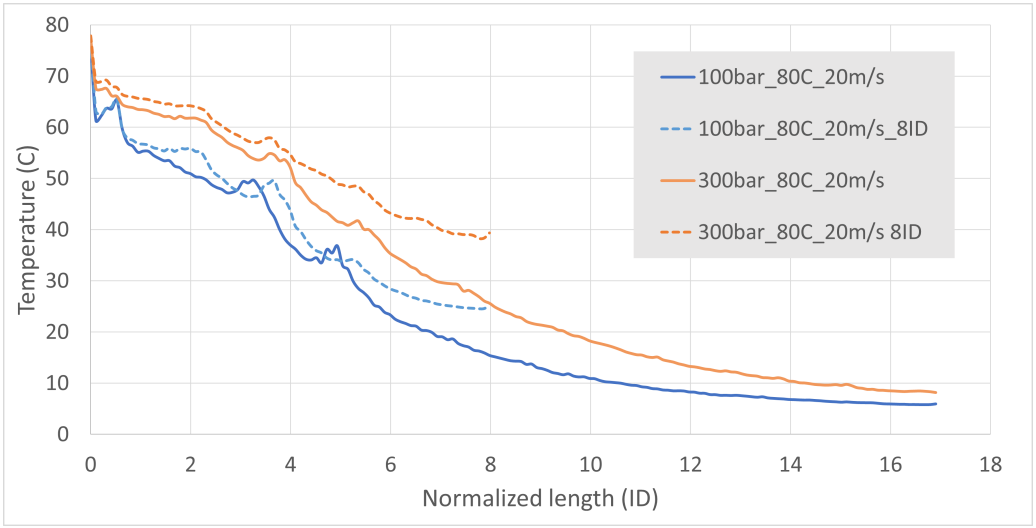

Figure 4.22: Compares temperatures for two different locations of the MEG surface. Solid lines represent 17 ID and dashed ones 8 ID. Same color represent same operating condition.

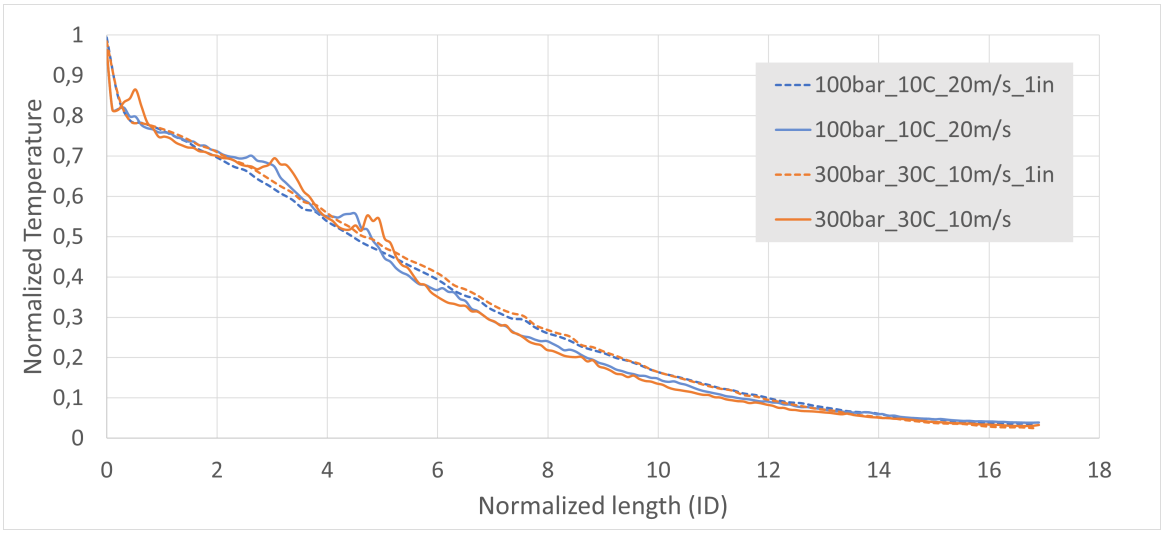

Figure 4.23: Compares different small bore diameters. Same color indicate the same operating conditions.

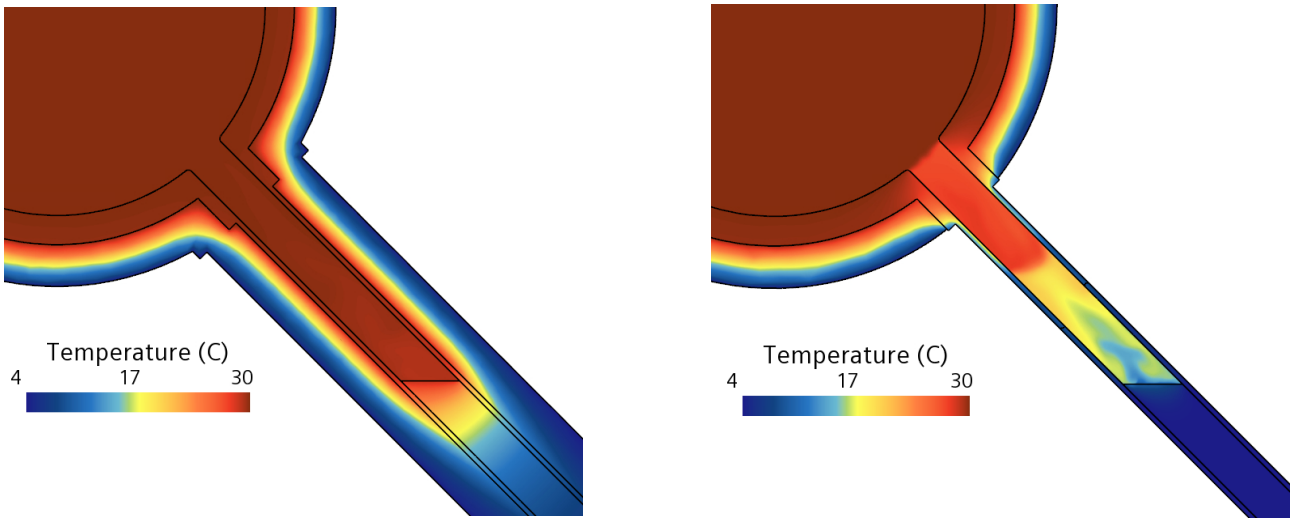

(a) Insulated

(b) Uninsulated

Figure 4.24: Effect of insulation on small bore piping

5
Discussion

In this chapter the results are discussed, like other chapters the two parts of the thesis are handled separately. Firts, the results of the hydrate modelling using CFD is discussed. Secondly the results of the thermal CFD analysis are discussed.

5.1 Hydrate modelling in CFD

There are two major uncertainties in the CFD set-up trying to replicate the results of Rao et al. [13]; how large the cooling line through the steel pipe was and how large the IHTC and EHTC were. The CFD model used a rather thick walled steel pipe while a better choice might have been a thin-walled pipe. Thinner walls would give a larger area for heat exchange between coolant line and steel pipe resulting in pipe temperatures closer to the coolant temperature.

The heat transfer coefficients are uncertain since they were implemented into the CFD solution based on a misunderstanding of where the calculated HTC's in the paper were located. However, calculating a new IHTC to be used in the CFD simulation was not certain to improve the reuslts since no velocity was specified for the coolant line.

The final thickness obtained in experiments was observed to be uniform but it is not specified in what plane the thickness was measured. The thickness might very well be uniform in the axial direction (horizontal plane). However, it is reasonable to believe that the hydrate thickness is larger on the bottom side of the steel pipe than the top (vertical plane) due to natural convection. Due to the low velocities in this case, natural convection will have a significant impact.

All CFD methods evaluated are based on the assumption of a gas dominated flow since they grow hydrates from the cold pipe surface rather than forming smaller hydrate particles that agglomerate and deposit downstream as oil dominated flows tend to do. The models consider the possibility of hydrates being torn from the wall due to shear stresses into account either. However the CFD methods developed should be fairly accurate for small bore dead legs in gas dominated flows where velocities (and shear stresses) are small.

5.1.1 Numerical resistance

This method was easily implemented with a low computational cost. The main drawback of the method is that it over-predicts hydrate thickness. Since it doesn't take into account the smaller cross-sectional area of the fluid channel as the hydrate grows the method is best suited for predicting thin hydrates that don't significantly change the cross-sectional area of the pipe.

This method may have some use as a conservative prediction for hydrate thickness in cases where the hydrate layer is relatively thin compared to the pipe diameter.

5.1.2 Surface wrapping

The main problem with the surface wrapping method was difficulties in meshing the new wrapped region. The wrapped region was specified to be any gas with temperature below HFT. Since this cold gas starts as a thin boundary layer next to the pipe the wrapped region is a thin shell which is troublesome to mesh in a proper manner. A possible remedy for these meshing problems would be to initialize a thicker cold region at the start and wrap it to have a thicker region to mesh. This was however not pursued further since the method would require too much customization for each case.

5.1.3 VOF with Melting-Solidification

This was seen as the most promising method and therefore the one most effort was put into. The main drawback for the method compared to the others was the computational cost as this was needed to be run transient.

AMR enabled the use of small cells at the interface between hydrate and gas while still keeping the number of cells acceptable. Cell size could be seen to have a large impact of how thick the hydrate grew why keeping small cells at the interface was essential. Two refinement levels was seen as a good compromise between accuracy and cost since the number of cells are increasing rapidly with additional refinement levels while the thickness change decreases.

Comparing case 2 and 3 shows that the CFD model is more sensitive to the water bath temperature than the experimental cases were. Since the water bath temperature was the only parameter varied between these cases it suggests that the EHTC used in the CFD simulation is too large. Since there was no active mixing in the water bath a low EHTC is feasible.

The same reasoning can be applied to the IHTC. The CFD results from case 2 and 3 show larger sensitivity to coolant temperature than the experiments. Thus both the IHTC and EHTC might need to be lowered to acquire a model able to predict hydrate thickness accurately.

It is hard to directly compare the CFD results with the experimental ones since the CFD used a surface average of the hydrate thickness around the whole steel pipe while the experimental results only looked at a single point. The resulting thickness from the CFD simulations were quite uniform in the axial direction but varied greatly in the circumferential direction. Clarifications regarding point of measurement in the experiments should be made before any other alterations of the model are done.

In summary this VOF method has proven to have potential and should be further investigated and compared to more cases, preferably with thicker hydrate layers. A greater thickness would reduce the influence of measurement errors in the experimental cases and would determine whether deviations from experimental results are of a absolute or relative nature.

5.2 CFD thermal analysis

The chosen models in the CFD thermal analysis includes relevant physics for obtaining reliable results in terms of temperature fields in the domain. This includes resolving the heat transfer in the fluids, piping and valve steel as well as the insulation. As described in section 3.3.3, the fluid is represented with temperature varying properties. This should increase the accuracy of the results, mainly in terms of resolving any natural convection occurring in the system. Areas that could be expanded upon in the CFD thermal analyses are the external heat transfer from the insulation to the surrounding sea water, resolving the fluid flow in the MEG when included in MEG-lock designs as well as geometry details such as valve design, valve support interface and piping rounded edges.

The external heat transfer from the insulation to the surrounding sea water could be expanded upon by including and resolving the convection in the sea water. However, this would drastically increase the domain size of the simulations and thus increase simulation cost and time. The benefit of doing this is also debatable, as it is clear from Eq. 2.4 that for an increasing EHTC value the thermal resistance tends to zero. The dependency on EHTC therefore decreases as the value increases, and so any error in estimating EHTC at high values has little impact on the solution.

Regarding treating the stagnant MEG in MEG-lock design as a solid as opposed to a fluid, the physical phenomenon being neglected by this approach is the natural convection in the MEG caused by density variations due to temperature gradients. This is in fact a non-conservative approach since the natural convection in the MEG should increase the heat transfer between the MEG and the process fluid. The full extent of this neglected heat transfer is unknown, however conservative measures has been taken in almost all other aspects of the modelling and the designs in question are not operating on the edge of reaching HFT in the small bore dead leg. Therefore, the approach is deemed viable because of the upsides regarding simulation cost and time.

The geometry in the CFD simulations could be expanded up on by including detailed valve geometries. For example seals, spindles and other parts of ball valve can be constructed from different materials with different properties. However, since the results and recommendations for dead leg design are meant to be general, a simple and general approach is suitable. Therefore, the valves are represented by simple geometric shapes of typical overall dimensions. The choice to omit seals and similar parts of the valve should also be conservative as they are typically made from materials with a lower thermal conductivity and should thus provide some insulating effect. An area of uncertainty is the interface between the valve and the valve support. The heat transfer between the two parts will be dependent on the contact area and whether any barrier exists in between, e.g. any film or mat constructed in a lower heat conducting material placed between the valve and the valve support. For the analyses performed it is assumed that the entire bottom of the valve is in contact with the valve support and that no thermal barrier between the two is present.

As mentioned earlier, a conservative approach is taken to the thermal analyses when possible. This means that the operating conditions should provide a minimum value for when the designs

are expected to operate without hydrate formation. The operating conditions are conservative in terms of inlet temperature, mass flow and ambient temperature, which are arguably the most important external parameters for deciding the temperature field in the system. This means that any system operating at higher inlet temperature, mass flow or ambient temperature is expected to operate without hydrate formation in the dead legs evaluated and cleared in this project.

Regarding the risk of evaporation and dilution of MEG in MEG-lock HCD designs, it is clear that the risk increases with increasing main flow temperatures. Evaporation will be accelerated because of increased temperatures, and a greater amount of condensation will occur should the process fluid be cooled close to ambient temperature in the dead leg. The risk of hydrate formation relates opposite to temperature. This means that the dead leg design, and the insulation design in particular, should vary with process fluid temperature depending on which risk is of most concern. This particular problem does not necessarily fit the method and aim of this work, namely providing conservative lower limits of operating conditions for the designs. A better approach for this problem would be to investigate a larger range of operating temperatures and provide designs for sub-ranges that do not fall below HFT, while still not accelerating evaporation and condensation significantly.

5.2.1 Normalization of temperature profile

The normalization of temperature profiles along vertical, straight dead legs showed similar results for varying bore sizes and inlet temperatures. This is an indication that such a graph can be used to estimate the temperature profile in similar dead legs. However, it is important to note that many parameters that could impact the results have not been investigated and that the sample size and variation is small. Such parameters can include pressure and density variations, inlet mass flow, thermal properties of both fluid and other materials in the system or complex geometry variations. It is also unclear how larger temperature differences, i.e. large differences between ambient and inlet temperature, affect such a normalized curve. For the purpose of this thesis, the normalized graph should only be considered as an indication that it is relevant to provide recommendations on dead leg design in relation to normalized quantities, such as maximum length of a dead leg expressed in internal diameters.

5.3 V-bend

In this case the deadleg was not determined purely by the geometry of the pipe but also by how much MEG there was in the small bore. The amount of MEG in the small bore pipe could be reduced by either being flushed out or evaporated. Both of these mechanisms were affected by the operating condition. The effect of evaporation was not taken into account before a number of thermal simulations conducted with insulation had been run at the end of the project where it was realized that the MEG might evaporate. Due to lack of time no hot 80°C case was run with the multiphase set-up.

Preferably the initial multiphase simulation would also give the temperature field in the dead-leg. However due to convergence problems and challenges common to multiphase simulations, the decision was made to simplify the multiphase simulation and thereafter do a thermal single

phase simulation. Another reason for separating these two simulations was that the multiphase one needed be run transient. Attempts to perform it in a steady state case resulted in a smeared and fluctuating MEG/gas interface. Solving the temperature field in a transient framework would require to run the simulations for a much longer time. The decision to run two simplified simulations was seen as a good compromise to ensure that work could be completed on time.

5.3.1 Determining the MEG surface

The choice to use constant material parameters was necessary since temperature was not included in this simulation and thereby temperature dependent material properties couldn't be used. However, for this simulation there are good arguments that this choice will still give an acceptable level of accuracy in the simulation results. First, the velocities are not so large that compressible effects must be accounted for. Furthermore natural convection is not important when determining the MEG surface and would not flush out any MEG on its own. One adverse affect of the choice to use constant material properties is the impact of changing viscosity and density as the gas and MEG is cooled and heated respectively. As MEG is heated both density and viscosity will reduce, which should result in an increased amount of MEG flushed.

The dynamic pressure seems to be a good indication of how much MEG will be flushed out of the pipe. The logarithmic trendline fits the data fairly well, however the expression for the trendline should be used with caution and the trendline should be viewed more of an illustrative tool for highlighting the trend rather than an expression for predicting deadleg length.

Dynamic pressure is a function of velocity and density. Since density for the gas used is more dependent on pressure than temperature it is reasonable that our results are more sensitive to pressure and velocity than temperature. Therefore it was deemed acceptable that no 80°C case was run.

The good agreement for different small bore diameters enables the use of non-dimensional numbers in general guidelines. To ensure the MEG surface stays above the bend a small bore length of 8 ID would give a safety margin and account for insecurities with the results.

5.3.2 Thermal analysis of the resulting deadleg

In the ideal case an integration in time of evaporation rate would be done to acquire the amount of evaporated MEG which in turn gives where the MEG surface will be located. An example of how that equation could look like can be seen in Eq. 5.1 where E is the evaporated MEG, $\dot{E}$ evaporation rate, T temperature on the MEG surface, t time and p pressure.

$$E = \int_t \dot{E}(T, p)dt \tag{5.1}$$

However, as the temperature in turn is dependent on operating conditions as well as the location of the MEG surface, the work to evaluate the expression quickly mounts to a significant task. Therefore a more pragmatic approach was chosen, approximating a temperature where

the evaporation should be insignificant.

From experiments conducted at sea level pressure the evaporation rate of a 80% MEG-water mixture was found to be 0.08 mg/min at 30°C [18]. Applying this rate to the analyzed small bore sizes would result in that at 30°C 1 ID length of liquid evaporates in 930 days or 115 days for the 50 and 25mm diameter sizes respectively. The study also concludes that water evaporates more readily than MEG and that as the MEG concentration increases the evaporation rate declines. Thus as more liquid evaporates the rate at which it does so will decrease. Further considering the high pressures subsea gas systems operate at the evaporation will be further suppressed. Hence at 30°C the evaporation could be deemed insignificant.

The difference between the temperature curves of the shorter and longer cases requires caution when using the 17 ID curves for predicting temperature for different locations of the MEG surface. As the MEG surface approaches 17 ID the agreement of the two temperature curves should however improve.

The worst case (300bar, 80°C, 20m/s) resulted in a temperature of 40°C at a 8 ID dead leg length, as can be seen in figure 4.22. The shorter cases have a 50-60% higher temperature at 8 ID dead leg length compared to the longer cases. If the same increase in temperature from the longer to the shorter case is assumed at 10 ID dead leg length, the temperature would be at or below 30°C. Thus a small bore length of 10 ID would be sufficient for all relevant cases.

Colder operating conditions could make use of a short small bore pipe, especially if the dynamic pressure is low as the amount of MEG flushed out will be reduced as well.

6
Conclusion

In this chapter the conclusions from the work are presented. For the hydrate modelling some recommendations for future work are presented. In terms of design guidelines limiting values are presented for key parameters, as well as some best practices for design philosophy.

6.1 Hydrate modelling

The VOF melting-solidification framework shows potential to be able to capture final thickness for hydrates. Some work needs to be done and preferably a larger range of hydrate thicknesses should be examined to determine if our deviations are of an absolute or relative nature. Tweaking values for heat transfer coefficients and investigating coolant line size as well as measuring point for the thickness should be the first remedies if future work is done based on the experiments performed by Rao et. al.

The two other methods for hydrate thickness prediction showed less potential and the authors cannot recommend to pursue them further.

6.2 Design guidelines

In this section design guidelines are presented with key diameters in non-dimensional numbers to enable general usage.

6.2.1 Hydrocarbon displacement lines

With the results from the thermal CFD simulations some conclusions for best practices on HCD line design can be made. The conclusions should be considered valid under equal or more favourable operating conditions as outlined in section 3.3.1. More favourable operating conditions include higher temperatures and flow rates as well as thicker insulation. In general, the effective small bore dead leg length should always be made as short as possible. Effective length includes the total length of piping filled with process fluid that is not part of the main process piping.

The 90° bend design with a valve support is a suitable candidate for a standard design option. The dead leg in this design is short and is supplied with heat in both ends of the dead leg. It also has the benefit of having a valve support included, which would otherwise need to be

designed separately. As a general principle, an interface between the valve and the valve support which transfers heat well should be incorporated. A favourable insulation design includes a co-insulated package, meaning the valve, valve support and the dead leg all share the same external insulation surfaces.

Should the valve have to be placed in a vertical position, as shown in figure 3.9a, the dead leg should be made as short as possible without bends. At a maximum, the dead leg length should not exceed 10 internal diameters.

If the valve can not be placed in the vicinity of the main process pipe according to the recommendations given above, a MEG-lock design should be used. As a general rule the section of the dead leg that is filled with process fluid should be kept as short as possible. Similarly to the straight vertical pipe a maximum of 10 internal diameters can be recommended. However, caution should be observed to not create tight clearances between the dead leg and the main process pipe as well as the dead leg to itself. This can lead to troublesome or impossible insulation application. As a recommendation, the clearances between insulation external surfaces should be kept above 50mm. This is a particular concern when dealing with 25mm bore size dead legs since the smaller internal diameter may require smaller bend radii. This recommendation applies not only to MEG-lock HCD designs, but any piping design which requires insulation.

At high operating temperatures, caution should also be observed with regards to evaporation and dilution of MEG. Based on the results from this work, no general recommendations can be given on best practices for mitigating this problem in MEG-lock HCD designs.

6.2.2 V-bend

For the v-bend geometry the important design parameter is the length down to the bend. This length should be long enough to ensure no gas reaches down to the bend and can propagate further through the small bore pipe. Ideally MEG in the small bore pipe will prevent this but two mechanisms can displace the MEG. First the dynamic pressure in the main pipe can flush out MEG, secondly the increased temperatures from the main pipe can evaporate additional MEG. A straight length of 10 ID of the small bore pipe is sufficient to prevent gas from reaching the bend in all relevant cases. For colder operating conditions this length could be decreased.

Bibliography

[1] R. E. James III, D. Kearins, M. Turner, M. Woods, N. Kuehn and A. Zoelle, "Cost and Performance Baseline for Fossil Energy Plants Volume 1: Bituminous Coal and Natural Gas to Electricity", NETL, Pittsburgh, PA, USA, NETL-PUB-22638, Sep. 2019.

[2] S. Varadhan and A. Sheldick. "COP26 aims to banish coal. Asia is building hundreds of power plants to burn it" reuters.com. https://www.reuters.com/business/energy/cop26-aims-banish-coal-asia-is-building-hundreds-power-plants-burn-it-2021-10-29/ (accessed May. 31, 2022).

[3] K. Mackarel and D. Michaels. "Nuclear Power, Natural Gas Secure EU Backing as 'Green' Investments" wsj.com. https://www.wsj.com/articles/nuclear-power-natural-gas-secure-eu-backing-as-green-investments-11643803487 (accessed May. 31, 2022).

[4] U.S. Energy Information Administration. "Natural gas explained" eia.gov. https://www.eia.gov/energyexplained/natural-gas/ (accessed Jan 24, 2022).

[5] J. M. Campbell, "Water-hydrocarbon phase behaviour" in *Gas conditioning and processing*, R. A. Hubbard, Ed., Norman, OK, USA: J. M. Campbell and Co., 2004, pp. 168-200.

[6] A. K. Sum, X. Zhang, J. H. Sa, B. R. Lee, T. Austvik, X. Li and K. M. Askvik, "Hydrate Management for Hydrate Deposition in Gas-Filled Vertical Pipes", presented at the Offshore Tech. Conf., Houston, TX, USA, 6-9 May, 2019, Paper OTC-29632-MS.

[7] Y. Bai and Q. Bai, "Subsea Field Development" in *Subsea Engineering Handbook*, Oxford, UK, Elsevier Science & Technology, 2012, pp. 22-23, 46-53.

[8] G. K. Anderson, "Enthalpy of dissociation and hydration number of methane hydrate from the Clapeyron equation," *J. Chem. Thermodynamics*, vol. 36, no. 12, pp. 1119-1127, Sep. 2004.

[9] D. Turner, "Clathrate hydrate formation in water-in-oil dispersions," Ph.D. dissertation, Dept. Chem. and Petro. Ref. Eng., Colorado School of Mines., Golden., CO, 2005.

[10] C. A. Koh, A. K. Sum and E. D Sloan, "Hydrate modeling and flow loop experiments for water continous and dispersed systems" Cent. for hydrate Res., Colorado School of Mines, Golden,USA, Doc. 10121-4202-01.02, 2012.

[11] F. Dorstewitz and D. Mewes, "The influence of heat transfer on the formation of hydrate layers in pipes" in *Int. J. Heat and Mass Transfer*, Vol. 37, No 14, pp. 2131-2137, 1994.

[12] J. R. Welty, C. E. Wicks, R. E. Wilson and G. L. Rorrer, "Fundamentals of heat transfer" in *Fundamentals of momentum, heat and mass transfer*, Hoboken, NJ, USA, Wiley & Sons, 2008, pp. 201-216.

[13] I. Rao, C. A. Koh, D. Sloan and A. K. Sum, "Gas Hydrate Deposition on a Cold Surface in Water-Saturated GasSystems" in *Industrial & Engineering Chemistry Research*, Washington DC, USA, American Chemical Society, 2013, Vol. 52, pp. 6262-6269.

[14] *Process Systems Design*, P-002, Standards Norway, Aug. 2014.

[15] *Hermetically Sealed Compressors*, MAN Energy Solutions, Accessed: May 17 2022, Available: https://www.man-es.com/oil-gas/products/compressors/sealed-compressor.

[16] F. Billard, D. Laurence, "A robust $k-\epsilon-\overline{v^2}/k$ elliptic blending turbulence model applied to near-wall, separated and buoyant flows" in *Int. J. of Heat and Fluid Flow*, Vol. 33, No 1, pp. 45-58, Feb. 2012.

[17] F. R. Menter, “Two-equation eddy-viscosity turbulence modeling for engineering applications” in *AIAA Journal*, Vol. 32, No8, pp. 1598-1605, Aug. 1994.

[18] M. Rusdi, Y. Moroi, H. Nakahara and O. Shibata, "Evaporation from Water-Ethylene Glycol Liquid Mixture" in *Langmuir*, Vol. 21, No. 16, 7308-7310, 2005.

A

Appendix A

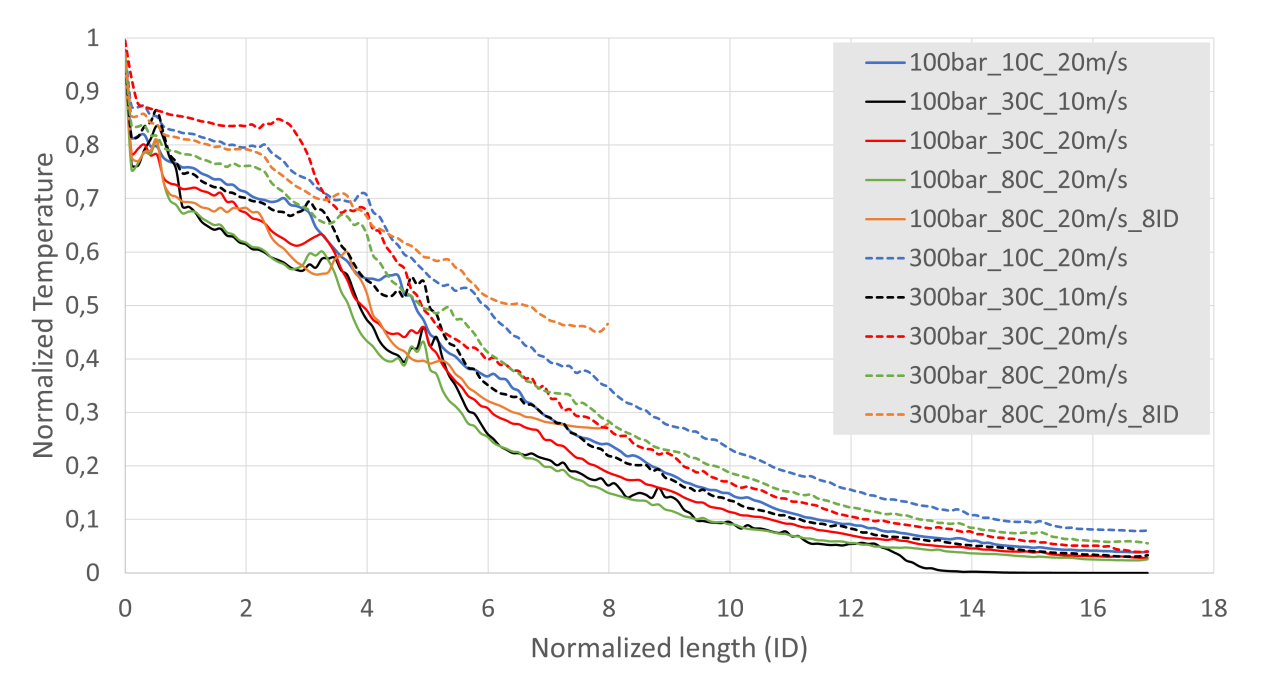

Figure A.1: Compares influence of different operating pressures. Lines of same color indicate same operating conditions except pressure.

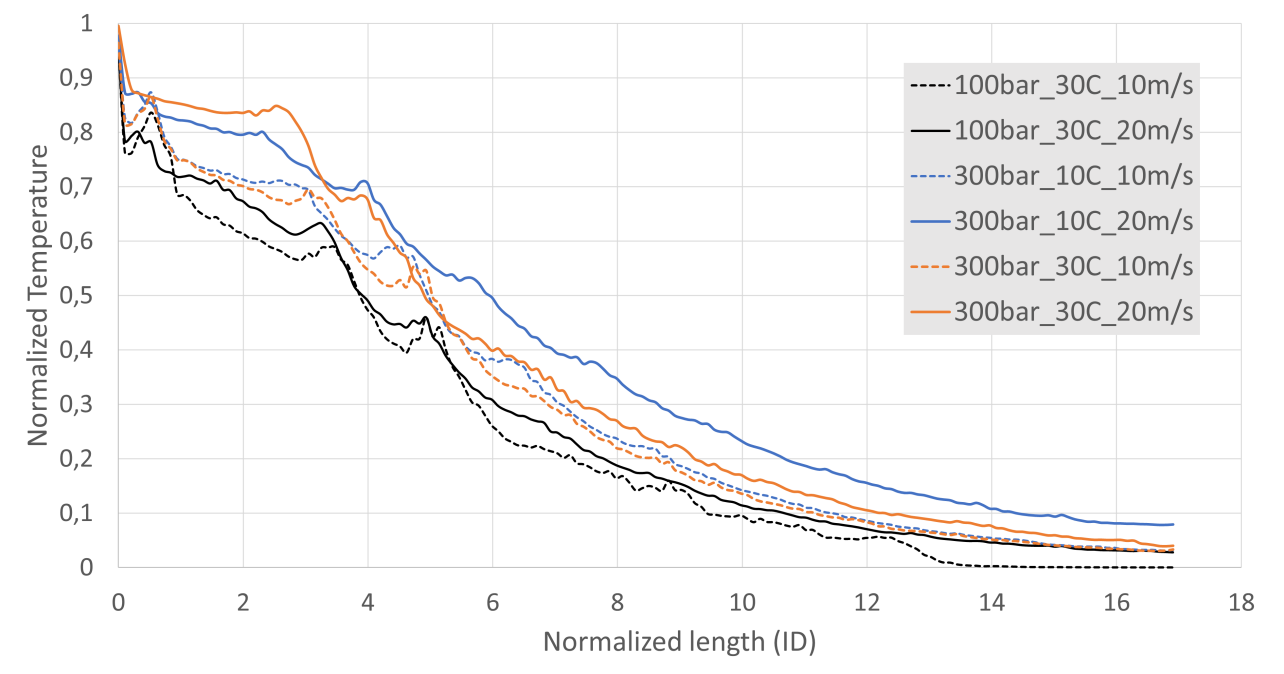

Figure A.2: Compares influence of different inlet velocities. Lines of same color indicate same operating conditions except velocity.

DEPARTMENT OF MECHANICS AND MARITIME SCIENCES
CHALMERS UNIVERSITY OF TECHNOLOGY
Gothenburg, Sweden
www.chalmers.se

CHALMERS
UNIVERSITY OF TECHNOLOGY